1

Quantum Dot Nuclear Spin Polarization

Patrick Maletinsky and Atac Imamoglu

[1] Institute of Quantum Electronics, ETH-Zürich, CH-8093 Zürich, Switzerland
patrickm@phys.ethz.ch
[2] Institute of Quantum Electronics, ETH-Zürich, CH-8093 Zürich, Switzerland
imamoglu@phys.ethz.ch

We present an all-optical study of the coupled electron-nuclear spin system in an individual, self-assembled quantum dot (QD). Nuclear spins are polarized by optical orientation of a quantum dot electron and subsequent transfer of angular momentum to the nuclear spins. We find the coupling between the electron and the nuclear spins to be highly nonlinear, leading to hysteresis of the nuclear spin polarization in external magnetic fields. Furthermore, we present a time-resolved study of the nuclear spin polarization where we show that the nuclear spin lifetime depends drastically on the charging state of the QD. If a single electron occupies the QD, nuclear spin polarization decays within a few milliseconds. This decay time is extended to a few minutes in the absence of the QD electron, indicating that the QD nuclei constitute a mesoscopic nuclear spin system which is very well isolated from its environment.

1.1 Introduction

The QD nuclear spin ensemble investigated in this work is addressed in experiments which consist of two basic steps. First, optical excitation of a QD with circularly polarized light is used to dynamically polarize the nuclear spins in the QD. Second, the nuclear spin polarization is detected by measuring the energy-shift of a QD emission line due to the effective magnetic field of the spin polarized nuclei.

When an electron spin system is driven out of thermal equilibrium through an external agent, electron spin relaxation drives the electrons back to a thermal state. Since this relaxation is partly happening via the nuclear spin reservoir, angular momentum is transferred to the nuclei and a net nuclear polarization can be established [1]. An efficient way of achieving this situation is optical excitation of spin polarized electrons in bulk semiconductors. Optically induced dynamical nuclear spin polarization (DNSP) was first demonstrated in silicon [2] and was later on studied extensively for nuclei close to paramagnetic impurities in GaAs [3].

Individual, optically active, self assembled QDs present an excellent system for studying optically induced DNSP in more depth, thereby revealing subtleties of the electron-nuclear spin system that were experimentally not accessible before. Several aspects distinguish the QD system from its bulk counterpart mentioned above: The narrow QD emission lines enable a direct measurement of electron nuclear interaction energy. This is not possible in bulk systems where typical widths of emission lines are an order of magnitude larger than the electronic energy shifts induced by polarized nuclei. In addition, the possibility of addressing a single QD has the advantage of removing effects of sample inhomogeneities and crosstalk between individual islands of spin polarized nuclei. Due to the different atomic composition and strain distribution of the QD as compared to its surrounding host material, the ensemble of $\sim 10^4 - 10^5$ QD nuclear spins can be considered as truly isolated from the environment. Therefore, the coupled electron-nuclear spin system of a QD is an implementation of a well isolated system of a single electron spin, coupled to a slowly varying, small nuclear spin reservoir, i.e., the central spin problem.

More recent interest in the dynamics of QD nuclear spins has arisen from the experimental and theoretical findings that the slow fluctuations of the nuclear spins constitute the dominant source of decoherence of QD electron spins. Since these fluctuations have long coherence times, the resulting electron-spin decoherence is non-Markovian and hence the evolution of the electron spin is highly complex [4–6]. Controlling the nuclear spin fluctuations, for instance by producing a substantial nuclear spin polarization or by performing a series of projective measurements on the nuclear spins [7], could potentially suppress this decoherence mechanism [8].

Optical orientation of QD nuclear spins has been demonstrated experimentally by a few groups [9–16]. However, the degree of DNSP achieved in these experiments has been limited to $\sim 10 - 20\%$ in low external magnetic fields and did not exceed 60% in high fields. In order to reach even higher degrees of DNSP, a detailed analysis of both the formation dynamics and the limiting factors of DNSP is required. Since DNSP is a balance between nuclear spin polarization by the QD electron and nuclear spin depolarization, a measurement of the corresponding timescales as well as an identification of the factors that influence the nuclear spin dynamics is of great interest and relevance. Inherent properties of the QD nuclear spin system, like the respective role of nuclear spin diffusion, quadrupolar interactions and trapped excess QD charges can be investigated using time-resolved measurements of the nuclear spins. Furthermore, experimental determination of the nuclear spin decay time directly yields the correlation time of the fluctuations of the Overhauser field along the axis in which the nuclei are polarized - a crucial quantity for understanding the limits of electron spin coherence in QDs [17].

In this work, we give an overview of our experimental assessment of the above mentioned points. After describing the sample investigated in this work and the experimental setup of our spectroscopy system in some detail in

Sect. 1.2, we give a short review of the theory essential for the interpretation of our experimental findings in Sect. 1.3. We then turn to our experimental results, starting with the low field behavior of DNSP in Sect. 1.4, where we describe the first measurement of the Knight field of a single electron confined to a QD. The nonlinear nature of the coupled electron-nuclear spin system is most pronounced in strong external magnetic fields, where DNSP may have a hysteretic response to the applied field, as we will show in Sect. 1.5. Finally, in Sect. 1.6 we focus on time-resolved measurements of DNSP, both in low and in high external magnetic fields. These measurements allowed us to identify the dominant nuclear spin relaxation mechanisms in self-assembled QDs which we discuss in detail at the end of this section.

1.2 Experimental Methods

The experimental results presented in this work have been obtained on individual, self assembled InAs QDs. These QDs have been embedded in gated structures that allow for deterministic QD charging with individual excess charges (electrons or holes) [18]. The sample was grown by molecular beam epitaxy on a (100) semi-insulating GaAs substrate. The InAs QDs are spaced by 25 nm of GaAs from a 40 nm doped n^{++}-GaAs layer, followed by 30 nm GaAs and 29 periods of AlAs/GaAs (2/2 nm) superlattice barrier layer, and capped by 4-nm GaAs. A bias voltage is applied between the top Schottky and back ohmic contacts to control the charging state of the QDs. The low density of QDs ($< 0.1\,\mu\mathrm{m}^{-2}$) allows us to address a single QD using a micro-photoluminescence (μ-PL) setup.

Our standard μ-PL setup is based on the combination of a ZrO_2 solid immersion lens in Weierstrass configuration, directly fixed onto the sample, and a PL collection lens of numerical aperture ~ 0.1 mounted outside the cryostat. Depending on the discussed experiment, the sample was placed either in a helium-bath cryostat equipped with a superconducting magnet, reaching a maximum magnetic field strength of 10 T, or in a helium flow cryostat. There, variable low magnetic fields of $B_{\mathrm{ext}} < 20$ mT or, alternatively, fixed magnetic fields of $B_{\mathrm{ext}} \approx 200$ mT were applied using external Helmholtz coils or a permanent magnet, respectively. In the case of the flow cryostat, the collection lens was replaced by a microscope objective with a numerical aperture of 0.26, resulting in an enhanced photon collection efficiency.

The spectroscopy system consists of a spectrometer of 0.75 m focal length and a liquid-nitrogen cooled charge coupled device (CCD) camera. The spectral resolution of this system is limited to ~ 30 μeV by the finite CCD pixel separation. However, the precision to which the emission energy of a given spectral line can be determined, can be increased to ~ 2 μeV, by calculating a weighted average of the emission line over the relevant CCD pixels [19]. Alternatively, by using a scanning Fabry-Perot interferometer of 62 μeV free

spectral range and a finesse ≥70 as a narrow-band frequency filter in front of the spectrometer, a spectral resolution < 1 μeV can be achieved [14].

The PL polarization and spin splitting are studied by resonantly exciting a single QD in one of its excited ("p-shell") states at T = 5 Kelvin. The PL spectral lines associated with different charging states of a single QD [18] can be identified from the PL intensity contour plot as a function of the bias voltage and emission energy (Fig. 1.1a). The emission line coming from neutral exciton (X^0) recombination exhibits a fine-structure splitting of ~ 20 μeV due to the anisotropic electron-hole exchange interaction (AEI) [20]. The emission from the negatively (positively) charged trion X^{-1} (X^{+1}) arises from optical excitation of QD charged with a single electron (hole). The photons emitted upon X^{-1} (X^{+1}) recombination are red (blue) shifted by ∼4.6 meV (∼1.9 meV) with respect to the X^0 line.

Unless stated otherwise, the discussed experiments have been performed on the negatively charged exciton X^{-1} at the center of its PL stability region with respect to gate voltage. In this regime, electron co-tunnelling to the nearby reservoir was shown to be minimized [21] and the QD is occupied by a single electron in its ground state. Optical excitation is performed in a resonant way into the "*p*-shell", which lies approximately one LO phonon energy above the emission energy of X^{-1} ($E_0 = 1.3155$ eV)[3]. The excitation power is fixed close to saturation of the observed emission line. We found that these conditions lead to a maximal preservation of PL light polarization ($|\rho_c^{\pm}| \approx 75\%$ at $B = 0$ T) after excitation with circularly polarized light.

The polarization of the excitation laser and of the PL are denoted as $(\sigma^\alpha, \sigma^\beta)$, where σ^α and σ^β are the excitation and detection polarization, respectively. The index α or β takes one of four values: linear polarization along the crystal axes ($x : [1\bar{1}0], y : [110]$) or circular polarization ($\pm$: light helicity ± 1). The degree of circular polarization is defined as $\rho_c^{\pm} \equiv (I^{\pm} - I^{\mp})/(I^{+} + I^{-})$, where I^β denote the intensity of PL in the $(\sigma^{\pm}, \sigma^\beta)$ configuration. The polarization characteristics of the system is calibrated using the strongly polarized emission of the LO phonon of the GaAs substrate (Fig. 1.1a) [23]. The combined fidelity of polarization preparation and detection was found to be better than 98%.

Circularly polarized, resonant p-shell pumping of a single electron (hole) charged QD generates optically oriented trions with hole (electron) spin $J_z = +3/2$ ($S_z = -1/2$) or $J_z = -3/2$ ($S_z = +1/2$), under σ^+ and σ^- pumping, respectively [12, 22]. The intra-dot excitation ensures maximal car-

[3] We exclude resonant ground state excitation by simultaneous LO phonon emission through various experimental observations: We observe several distinct QD excitation resonances at different energies. The GaAs LO phonon line for these resonances can thereby lie above or below the corresponding excitonic emission energy. The observed resonances have widths on the order of 100 μeV, in accordance with [22]. Only a few of these resonances lead to the high degree of PL circular polarization and to the nuclear spin polarization effects that will be discussed later. These facts corroborate or model of resonant excitation into the "p-shell".

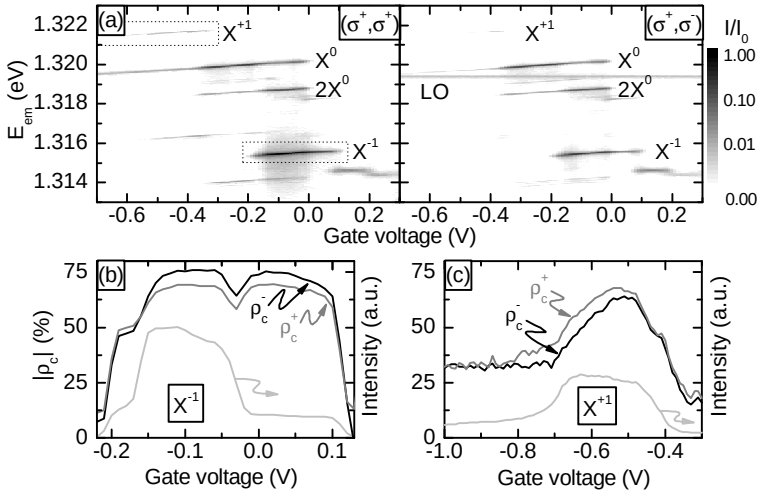

Fig. 1.1. Photoluminescence from a single charge-tunable QD. (a) Contour plot of the PL intensity as a function of applied bias voltage under circularly polarized excitation and co- (cross-) circularly polarized detection ($(\sigma^+,\sigma^{+(-)})$, respectively). The intensity is normalized with respect to the X^{-1} peak-intensity of $I_0 = 3 \cdot 10^4$ counts/sec. The excitation laser energy is tuned to a p-shell resonance of the singly charged QD at 1.356 eV, ∼36.6 meV above the bulk GaAs LO phonon line indicated in Fig. (a). Panels (b) and (c) show the integrated intensities of X^{-1} and X^{+1} emission in the (σ^+,σ^+) configuration (light gray), as well as the degree of circular PL polarization $\rho_c^{\pm}$ under $\sigma^{\pm}$ excitation. For (c), the laser is tuned into a p-shell resonance for X^{+1}

rier spin preservation during relaxation, which is confirmed by the high degree of circular polarization of the PL emission lines (Fig. 1.1(b) and (c)). The initial state of X^{+1} is composed of two holes in a singlet-state and one electron. Therefore, σ^+ (σ^-) polarized PL from X^{+1} indicates that the optically created electron was in the $S_z = -1/2$ ($S_z = 1/2$) state. Analogously, for X^{-1}, circular polarization of the emitted light reflects both the spin of the hole in the QD before photon emission and the initial spin of the residual QD electron after photon emission. A high degree of circular polarization of X^{-1}-emission thus indicates a highly spin polarized residual electron in the QD.

1.3 Electron and Nuclear Spin Systems in a Single Quantum Dot and Implications for Electron Spin Coherence

Circularly polarized excitation and the analysis of PL light polarization are powerful experimental tools for manipulating and measuring the spin polarization of the electron spin system in a single QD. The high degree of QD

PL polarization described in Sect. 1.2 indicates that electron spin relaxation mechanisms in the investigated QDs are relatively weak. Since the electron spin system is in thermal contact with the nuclear spin system through the hyperfine interaction, spin polarization is transferred from one to the other, thereby cooling the nuclear spin system. At the same time, the coupling of the nuclear spins to their environment will heat up the nuclear spins, leading to a finite nuclear spin temperature in a dynamical equilibrium. In this section, we give an overview of the basic spin interactions and relaxation mechanisms of the QD electron and nuclear spins and discuss the coupling mechanism between the two spin systems. Finally, we discuss how this coupling effects the coherence properties of the electron spin.

The total Hamiltonian $\hat{H}$ for the electron-nuclear spin system can be written as[4]

$$\hat{H} = \hat{H}_{\mathrm{Z}}^{\mathrm{el}} + \hat{H}_{\mathrm{Z}}^{\mathrm{nuc}} + \hat{H}_{\mathrm{dip}} + \hat{H}_{\mathrm{HF}}. \tag{1.1}$$

$\hat{H}_{\mathrm{Z}}^{\mathrm{el}}$ and $\hat{H}_{\mathrm{Z}}^{\mathrm{nuc}}$ denote the electron and nuclear Zeeman Hamiltonian, respectively, while $\hat{H}_{\mathrm{dip}}$ denotes the nuclear dipole-dipole interactions and $\hat{H}_{\mathrm{HF}}$ the hyperfine interaction, which couples the electron and nuclear spins. We will discuss the individual terms of this Hamiltonian in more detail in the following paragraphs.

1.3.1 Electron Spin System

The electron spin system considered in this work consists of a residual QD electron in the case of X^{-1} and of the (metastable) photo-generated QD electron in the case of X^{+1}. Information about the electron spin is obtained by measuring the circular polarization of PL light.

When placed in a magnetic field, the spin of a QD electron experiences the Zeeman interaction, described by the Hamiltonian

$$\hat{H}_{\mathrm{Z}}^{\mathrm{el}} = g_{\mathrm{el}}^{*}\mu_B \hat{\mathbf{S}}_{\mathrm{el}} \cdot \mathbf{B}, \tag{1.2}$$

where μ_{B} is the Bohr magneton, g_{el}^{*} the effective electron g-factor and $\hat{\mathbf{S}}_{\mathrm{el}}$ the electron spin operator ($\hat{\mathbf{S}}_{\mathrm{el}} \equiv \frac{1}{2}\hat{\boldsymbol{\sigma}}$, with the Pauli-matrices $\hat{\boldsymbol{\sigma}}$).

For a consistent notation with respect to the sign of the g-factors, we also note the Zeeman Hamiltonian for holes, which we write as $\hat{H}_{\mathrm{Z}}^{\mathrm{h}} = -g_{\mathrm{h}}^{*}\mu_B \hat{\mathbf{S}}_{\mathrm{h}} \cdot \mathbf{B}$ [24], with the effective hole g-factor g_{h}^{*} and the hole spin operator $\hat{\mathbf{S}}_{\mathrm{h}}$. In this representation, the heavy-hole wave functions $|\pm\frac{3}{2}\rangle$ convert to pseudo-spins $|\pm\frac{1}{2}\rangle$. The experimentally found g-factors g_{el}^{*} and g_{h}^{*} are both negative in our system.

Due to the tight confinement of electrons in self assembled QDs, the electron spin is well protected from spin-relaxation by electron-phonon coupling

[4] In this work, we only consider singly charged excitons. Exchange interactions therefore play no role for the energies of the recombining excitons [20].

via spin-orbit interaction, which is otherwise very effective in a solid state environment. This typically extends electron T_1 times in QD systems up to 1 s in moderate magnetic fields [25]. However, the coupling of the QD electron to the nearby electron reservoir introduces an additional - albeit controllable - decay channel for the electron spin. The QD electron can make a virtual transition to the Fermi sea of the reservoir and be replaced by a spin-flipped electron from the same reservoir. The rate of these co-tunneling events depends critically on the tunnel barrier between the QD and the electron reservoir and therefore in the details of the QD heterostructure. For the structures used in this work, the resulting T_1 time of the electron has an upper bound of ~ 3 ns at gate voltages in the center of the $1e^-$ stability region and decreases rapidly towards the edges of this region [26]. This tunability of the electron spin lifetime will be an essential feature in the measurements of the nuclear spin lifetime, as will be shown later.

1.3.2 Nuclear Spin System

The QDs considered in this work consist of InAs with an admixture of Ga due to material diffusion during the growth process. The nuclear spins present in our QDs therefore consist of three nuclear species with their naturally occurring isotopes: ^{115}In (95.3%), ^{113}In (4.7%),^{75}As,^{69}Ga (60.1%), ^{71}Ga (39.9%) - their natural abundances are given in brackets. Indium has a total spin of $9/2$ while all other nuclei have spin $3/2$. In the following, we will only consider the most abundant nuclear species for simplicity and neglect the at least $\sim 10\%$ admixture of Ga in our dots.

Each nucleus i is characterized by its spin I^i and the gyromagnetic ratio γ_i, describing the response to a static external magnetic field $\mathbf{B}$:

$$\hat{H}_{\mathrm{Z}}^{\mathrm{nuc}} = -\gamma_i \hbar \hat{\mathbf{I}}^i \cdot \mathbf{B}, \tag{1.3}$$

where $\hat{\mathbf{I}}^i$ is the (dimensionless) spin-operator of the ith nucleus. The gyromagnetic ratios for In and As are $\gamma_{^{115}\mathrm{In}} = 9.365$ MHz/T and $\gamma_{^{75}\mathrm{As}} = 7.315$ MHz/T.

Interactions of nuclear spins dominate their energy spectrum at low magnetic fields and lead to spin-transport in high fields. The simplest, and in semiconductors usually dominant nuclear spin-spin interaction is the dipolar coupling between two nuclear spins i and j. It can be written as [27]:

$$\hat{H}_{\mathrm{dip}}^{i,j} = \frac{\mu_0 \hbar^2 \gamma_i \gamma_j}{4\pi r_{ij}^3} \left(\hat{\mathbf{I}}^i \cdot \hat{\mathbf{I}}^j - 3 \frac{\left(\hat{\mathbf{I}}^i \cdot \mathbf{r}_{ij}\right)\left(\hat{\mathbf{I}}^j \cdot \mathbf{r}_{ij}\right)}{r_{ij}^2} \right), \tag{1.4}$$

where $\mathbf{r}_{ij}$ is the vector of length r_{ij} joining the two nuclei, and μ_0 is the permeability of free space. The dipolar Hamiltonian of the total nuclear spin system is then a sum over all nuclear spin pairs: $\hat{H}_{\mathrm{dip}} = \sum_{i<j} \hat{H}_{\mathrm{dip}}^{i,j}$.

A common decomposition of this Hamiltonian divides $\hat{H}_{\mathrm{dip}}^{i,j}$ into spin-conserving ("secular") and -non-conserving ("non-secular") parts [27]. While

the former are responsible for nuclear spin diffusion within the lattice, the latter can lead to depolarization of nuclear spins in low magnetic fields. The strength of the interaction $\hat{H}_{\mathrm{dip}}$ is usually characterized by a "local field" B_{loc}, which is the effective magnetic field generated on the site of a nucleus by its neighboring nuclear spins. For bulk GaAs, B_{loc} is on the order of 0.1 mT [3]. It can be shown that the non-secular terms of $\hat{H}_{\mathrm{dip}}$ only contribute to the evolution of the nuclear spin systems for magnetic fields $B_{\mathrm{ext}} \leq B_{\mathrm{loc}}$. Below these fields, the non-secular nuclear dipole-dipole interactions depolarize the nuclear spins very effectively on a timescale $T_2 \approx 10 - 100\ \mu$s[5].

Nuclear spin relaxation in III-V compounds has been experimentally investigated in detail using standard NMR techniques [29]. The resulting T_1 times in InAs and GaAs were on the order of 1000 s for Ga and As and roughly 200 s for In at a temperature of 4 K. These values however were shown to be limited by nuclear spin relaxation by paramagnetic impurities, a mechanism absent in individual QDs. The remaining relevant nuclear spin relaxation mechanism is quadrupolar relaxation. This process results from nuclear transitions induced by the coupling of the nuclear quadrupole moment to phonon-generated electric field gradients at the nuclear site. The corresponding phonon-induced relaxation rate scales with temperature as T^2 and dominates over the temperature-independent relaxation by paramagnetic impurities for $T > 20$ K. We therefore estimate the nuclear T_1-time in our QDs to be further reduced by 2 orders of magnitude compared to the reported values [29]. Even though the nuclear T_1-time could be reduced again by the strong lattice deformations in self-assembled QDs, we assume nuclear spin-lattice relaxation to be completely negligible for our experiments. The only remaining mechanism leading to a decay of nuclear spin polarization in a QD could be spin-diffusion out of the QD into the surrounding bulk material. The spin-diffusion constant in GaAs has been measured experimentally to be $D = 10^{-13}\ \mathrm{cm}^2\, s^{-1}$ [30]. The typical timescale for diffusion out of a QD with a diameter $d \approx 20$ nm is therefore $d^2/D \approx 1$ min. However, the different nuclear species and local lattice structure within the QD compared to its surrounding bulk material should further reduce the diffusion constant and increase the diffusion time. Experimental work on nuclear spin diffusion between quantum wells has shown that this reduction amounts at least to a factor of 10 [31].

[5] We note that this is not a decoherence process in the sense of loss of information from the nuclear spins to a reservoir, resulting in a decay of the off diagonal elements of the nuclear spin density matrix. Rather, due to nuclear spin-spin interactions, these elements all evolve at different frequencies spread over an energy interval $\Delta E \approx \gamma B_{\mathrm{loc}}$. Then, as far as the expectation values of observables are concerned, the off-diagonal elements of the nuclear density matrix can be taken equal to zero after a time $T_2 \simeq \hbar/\Delta E$ [28]. After this time, the nuclear spin state is fully described by its mean energy or equivalently, its nuclear spin temperature. The relaxation time of this nuclear spin temperature is denoted as T_1.

1.3.3 Hyperfine Interaction

The dominant contribution to the coupling between the electron- and the nuclear-spin systems originates from the Fermi contact hyperfine interaction. For an electron in a QD and in first order perturbation theory, this interaction can be written as [3, 4, 32]:

$$\hat{H}_{\rm hf} = \frac{\nu_0}{8} \sum_i A_i |\psi(\mathbf{R}_i)|^2 \hat{\mathbf{S}}_{\rm el} \cdot \hat{\mathbf{I}}^i, \tag{1.5}$$

where ν_0 is the volume of the InAs-crystal unit cell containing eight nuclei, $\psi(\mathbf{r})$ is the electron envelope wave function[6], and $\mathbf{R}_i$ is the location of the ith nucleus. $A_i = \frac{2}{3}\mu_0 g_0 \mu_{\rm B} \hbar \gamma_i |u(\mathbf{R}_i)|^2$ is the hyperfine coupling constant and g_0 the free electron g-factor. A_i depends on the value of the electron Bloch function $u(\mathbf{R}_i)$ at the nuclear site. For all the nuclei in our system it is positive and on the order of 50 μeV (i.e., $A_{\rm In} = 56$ μeV and $A_{\rm As} = 46$ μeV [33]). We note that only electrons in the conduction band couple to the nuclear spins through (1.5). For carriers in the valence band of *III-V* semiconductors, this interaction vanishes due to the p-type symmetry of $u(\mathbf{R}_i)$ [34].

With the identity $\hat{\mathbf{S}}_{\rm el} \cdot \hat{\mathbf{I}}^i = I_z^i S_z + \frac{1}{2}(I_+^i S_- + I_-^i S_+)$, where $S_\pm$ and $I_\pm^i$ are the electron and nuclear spin raising and lowering operators, respectively, (1.5) can be decomposed into two parts [35]: A dynamical part ($\propto I_+^i S_- + I_-^i S_+$), allowing for the transfer of angular momentum between the two spin systems, and a static part ($\propto I_z^i S_z$), affecting the energies of the electron and the nuclear spins.

The dynamical contribution leads to a thermal equilibration of the electron and the nuclear spin systems. Neglecting other spin relaxation mechanisms and polarization due to thermalization in the external magnetic field, the mean nuclear spin polarization $\langle I_z^i \rangle$ along the quantization axis z is linked to the electron spin polarization S_z through the Curie-law like relation [36]:

$$\langle I_z^i \rangle = I^i B_{I^i}(x), \quad \text{with} \quad x = I^i \ln\left(\frac{1+2S_z}{1-2S_z}\right). \tag{1.6}$$

B_{I^i} is the Brillouin function of order I^i. For small electron spin polarizations $S_z \ll 1/2$, (1.6) can be expanded to $\langle I_z^i \rangle = 4/3 I^i(I^i+1)\langle S_z \rangle$, while for $S_z \approx 1/2$, $\langle I_z^i \rangle = I^i$.

The static part of the hyperfine interaction leads to the notion of the "effective magnetic fields", either seen by the electron due to spin polarized nuclei (Overhauser field $\mathbf{B}_{\rm nuc}$), or by the nuclei due to a spin polarized electron (Knight field $\mathbf{B}_{\rm el}$). Here, we only consider their projection along the z-axis, which we denote as $B_{\rm nuc}$ and $B_{\rm el}$, respectively. The corresponding Knight field operator $\hat{B}_{\rm el}^i$ is

$$\hat{B}_{\rm el}^i = -\frac{1}{\hbar\gamma_i}\frac{\nu_0}{8} A_i |\psi(\mathbf{R}_i)|^2 \hat{S}_z. \tag{1.7}$$

[6] In our convention, $|\psi(\mathbf{r})|^2$ is normalized to $\frac{8}{\nu_0}$.

Its expectation value $B^i_{\rm el} = \langle S| \hat{B}^i_{\rm el} |S\rangle$ depends on the electron spin state $|S\rangle$ and on the exact location of the nucleus i. For a fully polarized electron bound to a shallow donor[7] in GaAs, the maximal value of $B^i_{\rm el}$ has been estimated to be 13 mT for Ga and 22 mT As. These values, however, are further reduced to $f_{\rm el}B^i_{\rm el}$ if the QD is occupied by a single electron only in a finite fraction $f_{\rm el}$ of the total measurement time [3].

Analogously, the Overhauser field operator can be written as

$$\hat{B}_{\rm nuc} = \frac{1}{g^*_{\rm el}\mu_{\rm B}} \frac{\nu_0}{8} \sum_i A_i \left|\psi(\mathbf{R}_i)\right|^2 \hat{I}^i_z, \tag{1.8}$$

with the expectation value $B_{\rm nuc} = \langle \mu| \hat{B}_{\rm nuc} |\mu\rangle$ for a given nuclear spin state $|\mu\rangle$. This effective field leads to a total electron Zeeman splitting in the presence of both nuclear and external magnetic fields:

$$\Delta E^Z_{\rm el} = g^*_{\rm el}\mu_{\rm B}(B_{\rm ext} + B_{\rm nuc}). \tag{1.9}$$

The electronic energy shift due to spin polarized nuclei ($\Delta E_{\rm OS}$) is referred to as the Overhauser shift (OS). For a fully polarized nuclear spin system in bulk InAs, the OS due to the In and As nuclei amounts to $\Delta E^{\rm In}_{\rm OS} = \frac{1}{2}\frac{9}{2}56\mu$eV= 126 μeV and $\Delta E^{\rm As}_{\rm OS} = \frac{1}{2}\frac{3}{2}46\mu$eV= 35 μeV, respectively.

Singly charged excitons are ideal candidates for a spectroscopic study of DNSP in QDs. In these charge complexes, exchange interactions between the carriers play no role [20] and the magnetic field dispersion of the spin splittings of excitonic recombination lines is solely due to Zeeman interaction of the spins with (effective) magnetic fields. For X^{-1}, the total Zeeman splitting of the PL recombination line thus amounts to

$$\Delta E^{\rm Z}_{X^{-1}} = -g^*_{\rm h}\mu_{\rm B}B_{\rm ext} - g^*_{\rm el}\mu_{\rm B}(B_{\rm ext} + B_{\rm nuc}), \tag{1.10}$$

where $g^*_{\rm el}$ and g^*_h are the electron- and hole g-factors, respectively.

Exciting the QD with linearly polarized light creates residual electrons in a superposition of spin up and down, resulting in no nuclear polarization and therefore in $B_{\rm nuc} = 0$. Thus, comparing the Zeeman splittings of X^{-1} under linearly- and circularly polarized excitation ($\Delta E^{\rm Z,lin.}_{X^{-1}}$ and $\Delta E^{\rm Z,\sigma^\pm}_{X^{-1}}$, respectively) gives a direct measure of $\Delta E_{\rm OS}$ and $B_{\rm nuc}$:

$$\Delta E_{\rm OS} = \Delta E^{\rm Z,\sigma^\pm}_{X^{-1}} - \Delta E^{\rm Z,lin.}_{X^{-1}} = -g^*_{\rm el}\mu_{\rm B}B_{\rm nuc}. \tag{1.11}$$

The analysis of the spin splittings for X^{+1} is analogous and will not be given here.

1.3.4 Hyperfine-Induced Electron Spin Decoherence

As we argued in Sect. 1.3.1, QD electron spins are well protected from relaxation and their evolution is governed by the Zeeman interaction of the electron

[7] With a Bohr radius of 10 nm - comparable to our QD confinement length.

with (effective) magnetic fields. Besides the externally applied magnetic field, the electron experiences the strong nuclear magnetic field B_{nuc} (cf. (1.8)). This field can attain values of several T for fully polarized nuclei and can therefore significantly contribute to the QD electron spin dynamics. If the nuclear spins are not explicitly prepared in a specific spin state, each nuclear spin points in a random direction and the mean nuclear spin polarization of the ensemble of nuclear spins is a random variable with a Gaussian distribution, having a width $\propto \sqrt{N}$. The fluctuating nuclear field can therefore be estimated to be $\Delta B_{\mathrm{nuc}} \simeq A/\sqrt{N} g^*_{\mathrm{el}} \mu_{\mathrm{B}}$, which is on the order of 10 mT for typical QD sizes with $N \approx 10^5$.

In low external magnetic fields, $B_{\mathrm{ext}} \approx \Delta B_{\mathrm{nuc}}$, the evolution of the direction of the electron spin is therefore mostly determined by its interaction with the nuclear spins. The transverse components of B_{nuc} with respect to the electron spin direction lead to coherent Larmor precession. Equivalently, the flip-flop terms in (1.5) drive transitions between the electron spin up and down states, thereby coupling these two states and defining a new quantization direction for the electron spins.

In a magnetic field $B_{\mathrm{ext}} \gg \Delta B_{\mathrm{nuc}}$, where the electron Zeeman splitting largely exceeds the hyperfine coupling strength with the random nuclear field, electron-nuclear flip-flop events become energetically forbidden and the components of the nuclear field transverse to B_{ext} can be neglected. However, the longitudinal components of the nuclear field fluctuations lead to a fluctuation of the energies of the electron spin states. This fluctuation in turn leads to a decoherence of the electron spin with a corresponding T_2^* time [32]:

$$T_2^* = \frac{\hbar}{g^*_{\mathrm{el}} \mu_{\mathrm{B}} \sqrt{2\Delta B^2_{\mathrm{nuc}}/3}}. \tag{1.12}$$

With $\Delta B_{\mathrm{nuc}} \approx 10$ mT, T_2^* is of the order of 3 ns, in accordance with recent transport measurements in a QD system [37]. We note that this apparent decoherence on a timescale T_2^* only comes from the fact that real experiments constitute an average of many measurements, each of which is realized under another nuclear spin configuration. In each run, the electron therefore has another Larmor precession frequency, which combined with the experimental averaging leads to an apparent damping of the electron spin precession. For a given nuclear spin state, however, the evolution of the electron-nuclear spin system is perfectly coherent as long as the direction and magnitude of the nuclear field are not altered. This averaging effect can be eliminated by using spin-echo techniques which unwind the effect of a static nuclear field on the electron spins. Under such conditions, the electron spin dephasing time in electrostatically defined QDs was found to be $T_2 \approx 1\,\mu$s at $B_{\mathrm{ext}} = 100$ mT - 2 orders of magnitude longer than T_2^* [37].

The remaining electron spin decoherence is a consequence of the evolution of the nuclear spin system and in particular of the z-component B^z_{nuc} of the nuclear field. This evolution was neglected in deriving (1.12) and the arguments leading to the finite T_2^* time were given based on the picture of the "frozen

fluctuations" of the nuclear field. In order to understand the pure dephasing processes for a QD electron (characterized by a time T_2), it is therefore necessary to understand the mechanisms which cause the evolution of ΔB_{nuc} and the timescale at which this evolution happens.

In Sect. 1.3.2 it was shown that nuclear spin lattice relaxation is negligible in the temperature range relevant to the experiments discussed here. The only interactions relevant for the evolution of the nuclear field are therefore the nuclear dipole-dipole interactions (1.4) and the hyperfine interaction with conduction band electrons (1.5). Their main effect in changing B^z_{nuc} are flip-flop processes between different nuclei (i and j), which change the nuclear field because the two coupled nuclei might have different interaction strengths with the electron spin (i.e., $|\psi(\mathbf{R}_i)|^2 \neq |\psi(\mathbf{R}_j)|^2$).

Nuclear dipolar interaction strengths are characterized by the local dipolar field B_{loc} (cf. Sect. 1.3.2). The evolution of a nuclear spin due to interactions with its neighbors therefore happens at a rate corresponding to the nuclear Larmor precession rate in the field B_{loc}, i.e., at ~ 10 kHz. For external magnetic fields exceeding the B_{loc}, the only relevant contribution for the evolution of B^z_{nuc} are the secular terms of the dipole-dipole interaction which lead to diffusion and re-distribution of the nuclear spins. The corresponding rate of change of B^z_{nuc} due to dipolar interactions is therefore further reduced. The time required to change a given nuclear field by a magnitude ΔB_{nuc} has been estimated to be $\sim 0.01 - 10$ s [38].

The role of the hyperfine interaction for the evolution of the nuclear spin system is twofold. First, the Knight field B_{el} of a QD electron leads to precession of the nuclear spins around the electron spin at a rate given by the nuclear Larmor frequency in a field B_{el}. Being on the order of 1 mT [14], the Knight field leads to nuclear spin evolution on timescales comparable to the corresponding estimates for the dipolar interactions. This evolution, however gets suppressed in external magnetic fields exceeding B_{el}, where electron-nuclear flip-flop processes vanish in first order. The second effect of the hyperfine interaction on the nuclear spins are electron-mediated, long ranged nuclear spin-spin interaction. This second order process termed "indirect interaction" consists of a virtual electron-nuclear spin-flip followed by a spin-"flop" of the electron with another nuclear spin. The resulting decorrelation time of the nuclear magnetic field has been shown to scale as $N^{3/2}\Delta E^{\mathrm{Z}}_{\mathrm{el}}/A^2$ for $A/\Delta E^{\mathrm{Z}}_{\mathrm{el}} \ll 1$ [39], with a rough estimate of 1 ms for $N = 10^5$, $A = 50$ μeV and $\Delta E^{\mathrm{Z}}_{\mathrm{el}} = 200$ μeV.

Calculating the electron spin dephasing rate caused by the slow but random nuclear field fluctuations occurring on a timescale of $\sim 100\mu$s turns out to be a difficult task [40]. This rate not only depends on the timescale of nuclear field fluctuations, but also on the correlations of these fluctuations as well as on the width of the initial nuclear field distribution. Still, attempts have been made to calculate this quantity including the interaction mechanisms discussed above [4, 41]. The results of these calculations lead $T_2 \approx 1 - 100$ μs, in rough agreement with experimental results [37].

Since most solid state systems contain nuclei with non-zero spin, the only way to further increase the electron spin coherence time is to manipulate the nuclear spins. The goal of such a manipulation is then to suppress fluctuations of the mean nuclear spin, thereby leaving the electron to interact coherently with a static nuclear field. Two methods for suppressing nuclear spin fluctuations have been proposed up to now. They involve creating a very high degree of nuclear spin polarization [4] or, alternatively, repeated projective measurements of the nuclear field [7], causing a "quantum Zeno effect" on the nuclear spins.

1.4 Optical Pumping of Nuclear Spins in Low Fields: The Role of the Knight Field

In low external magnetic fields, the evolution of the nuclear spin system is governed by the nuclear dipole-dipole interactions, characterized in strength by a local magnetic field B_{loc} (cf. Sect. 1.3.2). If the total magnetic field seen by the nuclei is smaller than B_{loc} , nuclear angular momentum is not a conserved quantity. Instead, the nuclear spins evolve into a highly entangled many body state due to their dipolar coupling. In order to observe any nuclear spin polarization, it is therefore necessary to apply a magnetic field exceeding B_{loc}. This fact has been observed experimentally in different QD systems [13, 42] as well as in various bulk NMR experiments [28]. Remarkably, in a situation of tight electron confinement, the Knight field B_{el} can attain values exceeding the local field B_{loc}, thereby "stabilizing" the nuclear spin polarization and allowing for the observation of nuclear spin polarization even in the absence of an externally applied magnetic field.

1.4.1 Nuclear Spin Cooling in the Knight Field of the QD Electron

Creating a Knight field strong enough to suppress the non-secular terms of the dipole-dipole interaction requires a sizable QD electron spin polarization. We realize this situation by exciting our QDs resonantly in one of their excited ("p-shell") states as described in Sect.1.2.

Figure 1.2a shows the emission spectrum of X^{-1} at zero external magnetic field obtained by using a scanning Fabry-Perot interferometer under linearly and circularly polarized excitation. Under σ^x-polarized laser excitation, no fine structure splitting is observed, confirming the absence of nuclear spin polarization. Exciting the QD with $\sigma^{\pm}$-polarized light, spin doublets with a ~ 13 μeV splitting appear. For X^{-1}, PL peaks that are co-circular with the excitation laser have lowest energy for both σ^+ and σ^- excitation (Fig. 1.2a), indicating that the direction of the effective magnetic field causing the observed splitting is determined by the direction of the QD electron spin. We therefore attribute the observed splitting to DNSP and further test this hypothesis by performing an analogous measurement using X^{+1} trion excitation

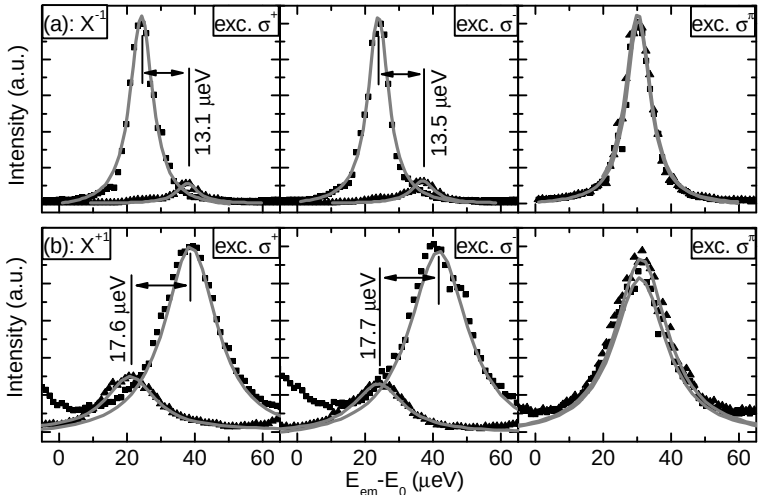

Fig. 1.2. Spin splitting induced by the Overhauser field. High-spectral-resolution PL spectra measured with a Fabry-Perot scanning interferometer (spectral resolution $\sim 1\,\mu$eV) under $B_{\rm ext} = 0$. The polarizations of the excitation laser are denoted in the figure. PL is detected co- and cross- polarized polarization with respect to the excitation (squares and triangles, respectively). Under circularly polarized excitation of X^- (a) as well as of X^{+1} (b), a significant nuclear spin polarization develops. In contrast, linearly polarized excitation does not lead to nuclear spin polarization. An energy offset of $E_0 \approx 1.3155$eV (1.3215eV) is subtracted from the X^- (X^+) data

(Fig. 1.2b). For X^{+1} , the observed energy sequence in PL emission is reversed, indicating that for a given excitation polarization the electron spin is polarized in opposite directions in the X^{-1} and X^{+1} trions [13]. This is consistent with the respective electron spin systems that were identified in Sect. 1.3.1.

Generally, the expectation value of the Overhauser field in a weak magnetic field B along the z-axis and and in the presence of nuclear dipolar interactions can be expressed as [3, 35, 36, 43]:

$$B_{\rm nuc} = f \frac{B^2 \langle S_z \rangle}{B^2 + \xi B_{\rm loc}^2}, \tag{1.13}$$

where $B = B_{\rm el} + B_{\rm ext}$ is the total effective magnetic field seen by the nuclei. $\langle S_z \rangle$ is the expectation value of the electron spin along the z-axis, ξ is a numerical factor of order unity and f is a proportionality constant determined by (1.6) and (1.8). The fact that we observe DNSP even if $B_{\rm ext} = 0$ suggests that the Knight field of a single spin-polarized electron is strong enough to ensure $B_{\rm el} > B_{\rm loc}$[8].

[8] We measured the stray field in our set-up to be 0.05 ± 0.01 mT at an angle of $\sim 25^\circ$ to the optical axis.

Based on (1.13), it could be concluded that application of an external field that cancels the Knight field should result in the complete disappearance of DNSP. Figure 1.3(a) shows the dependence of the observed Overhauser shift $\Delta E_{\rm OS}$ of X^{-1} on $|\mathbf{B}_{\rm ext}|$. A dip in the Overhauser shift at $B_{\rm ext} = -B_{\rm el} \approx \pm 0.6$ mT is observed under excitation with $\sigma^{\pm}$ polarized light, which gives a direct measurement of the average Knight field $B_{\rm el}$ experienced by the QD electrons. The direction of $B_{\rm el}$ is determined by the direction of the spin of the QD electron: Excitation with σ^{+} polarized light leaves a residual electron with spin up in the QD. Since $A > 0$, (1.7) implies that the Knight field indeed has to point in the negative direction.

Even when $B_{\rm ext} = -B_{\rm el}$, $\Delta E_{\rm OS}$ is only reduced from $\sim$ 16 μeV to $\sim$ 12 μeV, indicating that the cancellation of the Knight field $B_{\rm el}$ by the external field is not complete. The Knight fields we measured with this method range from ± 0.6 mT to $\sim \pm 3$ mT, depending on the degree of PL polarization, the excitation light intensity and the QD that was studied. The measured values indicate a time-averaged electron spin polarization between 3% and 30%. A fully polarized electron spin would have given rise to a Knight field on the order of $10 - 20$ mT (cf. Sect.1.3.3). Estimating the maximal value of $B_{\rm el}$ in a self assembled QD is difficult due to large uncertainties of the exact confinement length-scale and in the composition of the QD.

The principal reason for the incomplete reduction in DNSP at $B_{\rm ext} = -B_{\rm el}$ is the inhomogeneity of the Knight field. Since $B_{\rm ext}$ is homogeneous, the condition $B = 0$ is satisfied only for a small class of nuclei at any given $B_{\rm ext}$. The rest of the nuclei still experience a sizable total magnetic field and as a result, the Overhauser field is only slightly modified when $B_{\rm ext} = -B_{\rm el}$. To demonstrate the role of the inhomogeneous nature of the Knight field, we extended (1.13) to account for the inhomogeneity: We assume an in-plane Gaussian electron wave-function $|\psi(\mathbf{R}_i)|^2 \propto exp[-(x_i^2+y_i^2)/l^2]$ which we convolve with (1.13) to estimate the total contribution of the different classes of QD nuclei. The choice of a maximum Knight field of 1.5 mT in the center of the dot, $B_{\rm loc} = 0.11$ mT and $l = 20$ nm gives a reasonable description of the experimental data (solid curves in Fig. 1.3a), even though we only assumed a single nuclear species.

Remarkably, a minimum in the degree of PL polarization is also observed for the same $B_{\rm ext}$ where $\Delta E_{\rm OS}$ has a minimum (Fig. 1.3b): this is at first surprising since polarization of the X^{-1} trion line is solely determined by the hole-spin which has a negligible coupling to the nuclear spins. A possible explanation is based on AEI: after the resonant excitation of the QD, the electron excited into a p-shell state is expected to tunnel out into the n-doped GaAs layer in $\lesssim$ 10 ps [26]. After tunneling, the QD is neutral and the remaining electron-hole pair is subject to AEI which rotates the electron-hole spin [44]. This coherent rotation is then interrupted by re-injection of another electron from the n-doped GaAs layer into the QD s-shell to form a ground-state electron-singlet in $\tau_{\rm el} \approx 20$ psec, as required by the charging condition. Because tunneling is a random process, the time the QD spends in

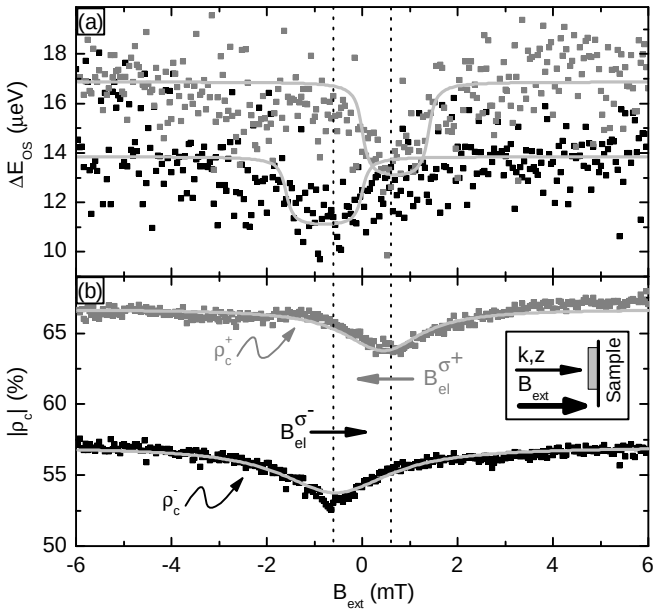

Fig. 1.3. Overhauser shift $\Delta E_{\rm OS}$ (a) and PL polarization (b) as a function of applied external magnetic field $B_{\rm ext}$. Here, the measured spin splitting is determined by a weighted average of the X^{-1} spectral lines measured by the spectrometer. The light gray curves in (a) and (b) are fits according to the model described in the text. Observation of correlated dips in spin splitting and in polarization as a function of $B_{\rm ext}$ suggests an average Knight field $B_{\rm el} \approx 0.6$ mT seen by the nuclei. Under σ^+ (σ^-) excitation, the corresponding Knight field $B_{\rm el}^{\sigma^{+(-)}}$ is parallel (anti-parallel) to the wave-vector $\mathbf{k}$ of laser excitation. The schematic in the inset of (b) sketches the orientations of the laser wave-vector and a positive external magnetic field

the neutral state is random and the post-tunneling hole-spin state is partially randomized, which leads to a finite ρ_c.

The Overhauser-field competes with the exchange interaction; a reduction in DNSP will therefore lead to a reduction in ρ_c as depicted in Fig. 1.3b. The PL polarization in the presence of an Overhauser shift $\Delta E_{\rm OS}$ and an exchange-splitting $\Delta E_{\rm ex}$ due to AEI can be approximated as [45]:

$$\rho_c = \frac{1 + \Delta E_{\rm OS}^2 \tau_{\rm el}^2/\hbar^2}{1 + (\Delta E_{\rm OS}^2 + \Delta E_{\rm ex}^2)\tau_{\rm el}^2/\hbar^2}, \tag{1.14}$$

provided other spin relaxation processes are neglected. Fitting the polarization $\rho_c(X^{-1})$ with the measured spin splitting in Fig. 1.3a, $\tau_{\rm el} = 30$ psec is obtained[9]. Below saturation, a reduction in the excitation power results in a

[9] As shown in Fig. 1.1b, the PL from this QD exhibits an asymmetric polarization under $\sigma^\pm$ pumping: the origin of this asymmetry is not clear and was not observed on all QDs studied.

decrease in both spin-splitting and ρ_c: this observation corroborates the model described by (1.14).

The electron (spin) exchange with the n-doped GaAs layer also explains how QD electron-spin pumping is achieved in a negatively charged QD: irrespective of the pre-excitation electron state, the sequential tunneling ensures that the QD ends up in a trion state where the electrons form an s-shell singlet. Preservation of hole-spin in these QDs then implies that the post-recombination electron is always projected into the same spin-state.

1.5 Bistability of the Electron Nuclear Spin System

DNSP behaves qualitatively different in low and high external magnetic fields. While the low field case was studied in the previous section, we now study a situation where the coupled electron-nuclear spin system is exposed to a magnetic field which is on the order of the Overhauser field B_{nuc}. There, the external magnetic field can fully compensate the nuclear field B_{nuc}, thereby greatly enhancing the electron nuclear spin coupling which depends on the effective Zeeman splitting of the electron spin.

In external magnetic fields, nuclear spin polarization manifests itself in a difference in emission energies between excitation with circularly and linearly polarized light as was established in Sect. 1.3.3. Fig. 1.4 shows the X^{-1} emission energies of a single QD under excitation with circularly polarized light as a function of external magnetic field. Gray (black) denotes excitation with σ^+ (σ^-) light, while squares (triangles) stand for co- (cross-) circular detection. The polarizations for excitation and detection are denoted as $(\sigma^\alpha, \sigma^\beta)$ where σ^α and σ^β correspond to excitation and detection, respectively. The data shown in Fig. 1.4 was obtained in a single sweep from $B = -2$ T to $B = +2$ T, varying excitation and detection polarization for each B-field value in the order $(\sigma^+, \sigma^-) \Rightarrow (\sigma^+, \sigma^+) \Rightarrow (\sigma^-, \sigma^+) \Rightarrow (\sigma^-, \sigma^-)$ such that any memory of the nuclear spin system is erased during the sweep. The data for $|B| < 500$ mT was taken with smaller magnetic field steps in order to highlight the detailed behavior of DNSP at low fields. Every data point represents the center of mass of the emission peak of X^{-1} taken from a single spectrum with 1 s integration time and a signal to noise ratio of $\sim 100 : 1$ for co-circular detection (Fig. 1.4b). The effects of nuclear polarization can be seen in the range of $|B_{\mathrm{ext}}| \lesssim 1.2$ T where emission energies for a given detection polarization depend strongly on the helicity of the laser light. Excitation with σ^+ light creates a residual electron with its spin pointing in the positive z-direction (see Fig. 1.4a). According to (1.5) and (1.8), this creates a nuclear spin polarization in the same direction and, due to the negative sign of the g^*_{el}, a nuclear field pointing in the negative z-direction. This scenario is consistent with the polarization sequences and lineshifts observed in Fig. 1.4c. Above 1.2 T, the emission energies of the QD are almost independent of excitation light polarization, indicating that nuclear effects become very small.

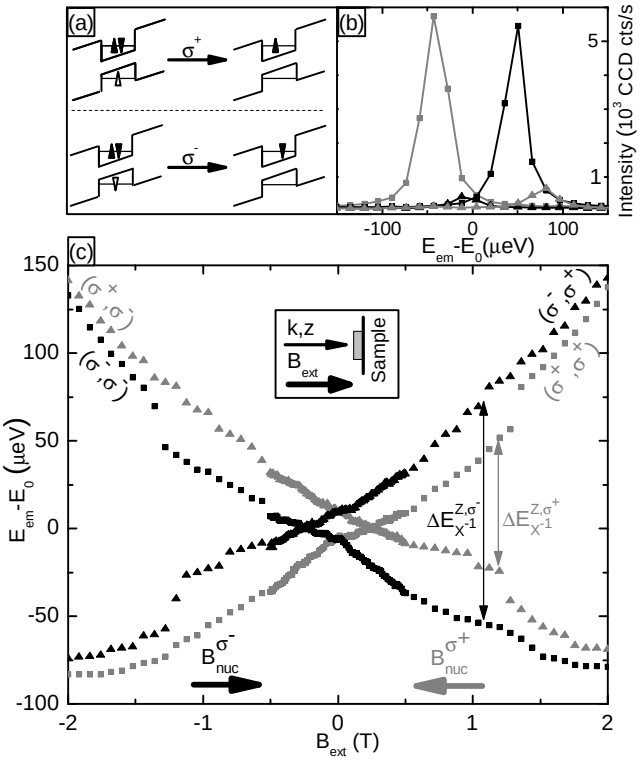

Fig. 1.4. (a) Configurations of X^{-1} before and after the emission of a $\sigma^{\pm}$ polarized photon. Open (filled) triangles denote the spin of the hole (electron). (b) Raw spectra at $B_{\rm ext} = -0.96$ T for the four excitation/detection configurations in the circular basis: gray (black) denotes excitation with σ^+ (σ^-) polarized light. Detection is co- or cross-circular (squares and triangles, respectively). (c) Energy dispersion of X^{-1} under circularly polarized excitation: The emission energies ($E_{\rm em}$) are different for σ^+- and σ^--polarized excitation due to DNSP and the resulting effective nuclear magnetic field $B_{\rm nuc}^{\sigma\pm}$ under $\sigma^{\pm}$ excitation (orientation indicated by the arrows in the figure). An energy $E_0 \approx 1.3155$ eV was subtracted from $E_{\rm em}$. The inset shows the relative orientation of k-vector, quantization axis z and positive magnetic field

Another striking feature in this data is the symmetry under simultaneous reversal of the excitation light helicity and the sign of the magnetic field. However, the data is not symmetric under the reversal of only one of these parameters. This asymmetry indicates that the system distinguishes between nuclear fields pointing along or against the external magnetic field - we will see in the following that it is more efficient for the system to create a nuclear field pointing against $B_{\rm ext}$ than one that points along this field.

In order to obtain a more quantitative picture of the magnetic field dependent DNSP, we performed the following analysis steps on the data (see Fig. 1.5): We first extract the Zeeman splittings for excitation with σ^+ and

σ^- light from the raw data shown in Fig. 1.4c. To this data, we fit a linear Zeeman splitting such that the fit coincides with the data at magnetic fields $B_{\rm ext} > 1.8$ T where nuclear polarization is very small (Fig. 1.5a). The excitonic g-factor, $g^*_{\rm ex} \equiv g^*_{\rm el} + g^*_{\rm h} = -1.87$ that we find with this fitting procedure matches within a few percent to an independent measurement of $g^*_{\rm ex}$ that we performed with linearly polarized excitation (not shown here). The Overhauser shift can now be extracted from this fit with the help of (1.11); the result is plotted in Fig. 1.5b. There is a striking difference when polarizing the nuclei along or against the external field. Nuclear polarization with $B_{\rm nuc}$ pointing along the applied field is rather inefficient and shows a slight decrease with increasing magnitude of the applied field. Polarization with $B_{\rm nuc}$ pointing against the external magnetic field on the other hand shows a much richer behavior: The nuclear polarization first increases almost linearly as the magnitude of the external field increases and then shows a sudden drop when $|B| \approx 1.2$ T. At $B = 0$, DNSP abruptly changes its dependance on magnetic field and $\mathrm{d}B_{\rm nuc}/\mathrm{d}B_{\rm ext}$ shows a sudden jump.

From the spectral data we can also extract information about the hole spin polarization before- and the residual electron spin polarization after recombination of X^{-1}. For this, we define a degree of QD spin polarization as $\rho_c^{\pm} \equiv (I_{(\sigma^\pm,\sigma^+)} - I_{(\sigma^\pm,\sigma^-)})/(I_{(\sigma^\pm,\sigma^+)} + I_{(\sigma^\pm,\sigma^-)})$ under $\sigma^\pm$ excitation. $I_{(\sigma^\alpha,\sigma^\beta)}$ are the intensities of the dominant PL-peaks in the corresponding analyzer/polarizer configurations. At $B_{\rm ext} = 0$, $\rho_c^{\pm}$ is equivalent to the PL circular polarization. At finite $B_{\rm ext}$ however, $\rho_c^{\pm}$ measures the relative weight of the two (perfectly circularly polarized) Zeeman split emission lines and is therefore a measure of hole spin preservation during relaxation from the p- to the s-shell. The measured quantity $\rho_c^{\pm}$ is plotted in Fig. 1.5(c) as a function of external magnetic field. It is roughly constant and on the order of 85% over a wide range of magnetic fields. Only for the fields where the trion Zeeman splitting vanishes due to a cancellation of the exciton Zeeman splitting with the Overhauser field, $\rho_c^{\pm}$ dips to roughly 65%. This behavior is consistent with the rotation of the exciton spin during relaxation of the optically created electron from the excited p-shell state to the s-shell via the electron reservoir (see Sect. 1.4.).

As in the data presented in Sect. 1.4, there is a certain asymmetry in the data shown in Fig. 1.5(c) that remains unexplained: ρ_c^- is larger than ρ_c^+ at high magnetic fields and the dip in ρ_c^+ at lower fields is less pronounced than for ρ_c^-. A possible reason for this asymmetry could be the different excitation efficiencies in the QD for σ^+ and σ^- excitation.

1.5.1 Modelling of the Data

Most of the above-mentioned nuclear effects in the presence of an external magnetic field can be described by a simple rate equation model proposed earlier [13, 32, 42] and originally based on work by Abragam and D'yakonov

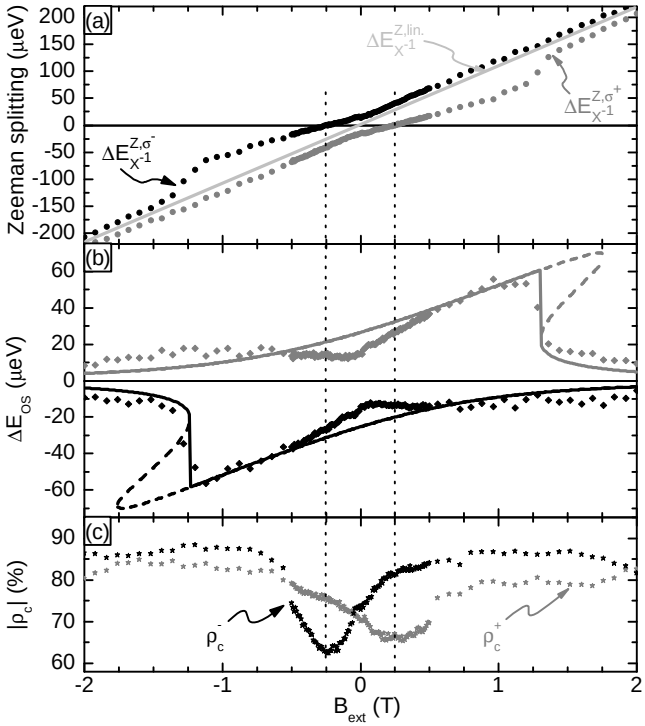

Fig. 1.5. Nuclear Polarization in external magnetic fields: (a) Spin splitting of X^{-1} under circularly polarized excitation. Gray and black symbols correspond to excitation with σ^+- and σ^--polarized light, respectively. The solid line is a linear fit to the data as described in the text. (b) Deviation of the spin splitting between circular and linear excitation: Overhauser shift for σ^+- and σ^--excitation (gray and black diamonds, respectively). The solid and dashed lines are the results of the fits according to the model discussed in the text. (c) QD spin polarization $\rho_c^{\pm}$ under $\sigma^{\pm}$ excitation extracted from PL intensities as described in the text. The polarization shows a minimum at the magnetic field where the exciton Zeeman splitting is zero, consistent with our model of carrier relaxation (Sect. 1.4)

[27, 46]. The rate equation is based on the condition for dynamical equilibrium (1.6) between the electron and the nuclear spin system in the absence of any coupling to the environment. This equilibrium is then reached on a typical timescale given by the nuclear spin relaxation time T_{1e}, which can be estimated to be [35]

$$\frac{1}{T_{1e}} = \frac{1}{T_{1e}^0} \frac{1}{1 + \Omega_{el}^2 \tau_{el}^2}. \tag{1.15}$$

Here, τ_{el} is the electron spin correlation time which broadens the electronic spin states. $\Omega_{el} = \Delta E_{el}^Z / \hbar$ is the electron Larmor frequency which depends on the degree of nuclear polarization through (1.8) and (1.9). For a given nuclear species, the nuclear spin relaxation time at zero electron Zeeman splitting is

given by $1/T_{1e}^0 = f_{el}\tau_{el}(A_i/N\hbar)^2$ with N the number of relevant nuclei and f_{el} the fraction of time the QD is occupied with a single electron. The quantity $A_i/N\hbar$ corresponds to the precession frequency of a nuclear spin in the Knight field of the QD electron. The expression for T_{1e}^0 is valid for $A_i/N\hbar \ll \tau_{el}^{-1}$ and if we assume a homogenous electron wave function $\psi(\mathbf{r}) \propto \sqrt{8/\nu_0 N}$ which is constant within the QD volume and zero outside.

By adding a nuclear spin decay channel which is dominated by nuclear spin diffusion out of the QD on a timescale T_d, we end up with a rate equation of the form

$$\frac{d\langle I_z^i\rangle}{dt} = -\frac{1}{T_{1e}}(\langle I_z^i\rangle - I^i B_{I^i}(x)) - \frac{1}{T_d}\langle I_z^i\rangle \tag{1.16}$$

$$\simeq -\frac{1}{T_{1e}}(\langle I_z^i\rangle - I^i) - \frac{1}{T_d}\langle I_z^i\rangle. \tag{1.17}$$

Due to the high degree of electron spin polarization deduced from the high value $\rho_c^{\pm}$, we expanded (1.6) to first order around $S_z = 1/2$ to arrive at (1.17).

This equation was obtained for the coupling of a single electron to a single nuclear spin. It can be approximately generalized to the case of an ensemble of different nuclei in the QD by considering the mean nuclear spin polarization $\langle I_z\rangle = \frac{1}{N}\sum_i \langle I_z^i\rangle$. For this, we replace the hyperfine constant A_i in (1.15) by the sum A, and the nuclear spin I^i in (1.17) by the average $\overline{I^i}$ over the two dominant nuclear spin species. With the values for A_i and I^i noted in Sect. 1.3.3, this results in $A = A_{In} + A_{As} = 102\ \mu$eV and $\overline{I^i} = \frac{6}{2}$. We take these numbers to be fixed in the following, even though the In content varies drastically within a QD and accurate estimates of $\overline{A_i}$ and $\overline{I^i}$ are difficult to obtain.

We note that this model was previously applied to situations where DNSP was induced by neutral excitons [32, 42]. There, anisotropic exchange interaction plays a crucial role and has to be included in the detuning factor in (1.15). In this work however, DNSP is induced by a single, spin-polarized electron for which exchange interaction plays no role[10].

Since the electron-mediated nuclear spin relaxation time T_{1e} itself depends on nuclear spin polarization, (1.17) leads to the following self-consistent non-linear steady state solution $\langle I_z^{ss}\rangle$ for the mean nuclear spin polarization:

$$\langle I_z^{ss}\rangle = \frac{\overline{I^i}}{1 + \frac{T_{1e}^0}{T_d}(1 + (\frac{\tau_{el}}{\hbar})^2(g_{el}^*\mu_B B_{ext} + A\langle I_z^{ss}\rangle)^2)}. \tag{1.18}$$

We note that averaging (1.17) over the different nuclear species, our choice of a homogenous electron wavefunction and the fact that we neglected the magnetic field dependence of T_d can all limit the validity of this model.

[10] We can rule out the possibility that DNSP is induced by the intermediate state where the QD is neutral during electron relaxation through the reservoir. In this case the direction of the nuclear field would be opposite to the one observed in the experiment.

In order to fit our experimental data, we numerically solved the implicit equation (1.18). The result of such a fit is shown in Fig. 1.5(b). The model qualitatively reproduces the data. Still, some features, like the before-mentioned kink of DNSP around zero external field as well as the high residual spin polarization at high external magnetic fields, could not be explained within the model or any reasonable extension [42] to the rate equation picture employed here. In the region 1.2 T$< B_{\mathrm{ext}} <$ 1.8 T the model predicts three solutions: two stable states, one with a low and one with a high degree of DNSP and an unstable solution of intermediate nuclear spin polarization (the last two solutions correspond to the dashed lines in Fig. 1.5). Since in this experiment we changed excitation polarization from σ^+ to σ^- for each magnetic field value, the system always followed the solution with minimal nuclear spin polarization. The fact that the drop in DNSP in this measurement was rather smooth compared to the model prediction was probably due to the long timescale of the buildup of DNSP right before its disappearance: since in the experiment every point was taken with an integration time of 1 s, the nuclear system did not have time to reach its steady state polarization before the excitation light polarization was switched. The parameters used for the fitting curve in Fig. 1.5(b) were $T_{1\mathrm{e}}^0/T_{\mathrm{d}} = 3.4$,$\tau_{\mathrm{el}} = 35$ ps, $g_{\mathrm{el}}^* = -0.69$, which are all realistic values for our QD.

The electron spin correlation time found in the fit can be explained with the resonant excitation scheme that we used in our experiments. The QD is excited from its ground state into the *p*-shell and after relaxation through an intermediate neutral excitonic state PL emission is observed from carriers recombining from the *s*-shell. Since this system is pumped close to saturation, the lifetime and thus the correlation time of the residual electron are limited by the relaxation time from the *p*-shell to the n^{++}-GaAs layer by tunnelling. This timescale is expected to be on the order of 10 ps and the value of 35 ps we find here is in good agreement with the value found independently in Sec. 1.4.

The parameters obtained in this fit also allow us to estimate the nuclear spin relaxation time $T_{1\mathrm{e}}^0$. Using the value $\tau_{\mathrm{el}} = 35$ ps, the corresponding value for $f_{\mathrm{el}} = 0.035$ (assuming an exciton lifetime of 1 ns) and N$= 10^4 - 10^5$, we obtain $T_{1\mathrm{e}}^0 = 1 - 100$ ms.

1.5.2 Hysteresis in the Magnetic Field Sweeps

In this section, we focus on the bistable behavior of the coupled electron-nuclear spin system in the magnetic field range close to the "breakdown" of DNSP. Fig. 1.6(a) shows a graphical representation of the solutions of the nonlinear equation (1.18). The result suggests that the maximal achievable degree of DNSP in our system leads to a maximal OS given by $\mathrm{OS}_{\mathrm{max}} = A\overline{I^i}(1+T_{1\mathrm{e}}^0/T_{\mathrm{d}})^{-1}$. This value is reached when nuclear spin relaxation is maximized, i.e., when the total electron Zeeman splitting is zero (cf. (1.15)). It can also be seen from the figure that there is a regime of external magnetic fields where two stable solutions for DNSP coexist. One solution leads to a

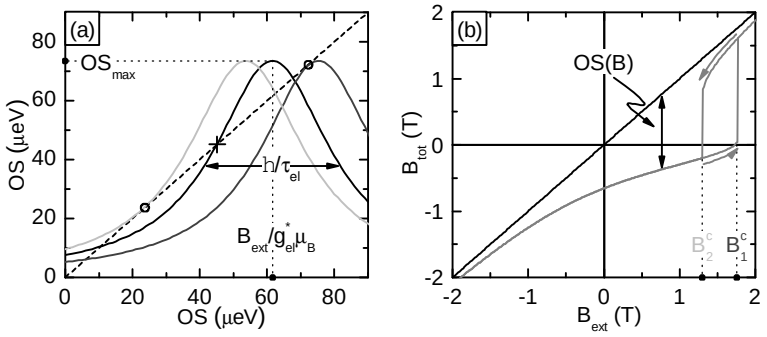

Fig. 1.6. (a) Graphical solution of (1.18): The right (left) hand side is represented by the solid curves (dashed line). These terms correspond to gain and loss of DNSP, respectively. Circles (cross) indicate the stable (unstable) solutions for nuclear spin polarization. The center of the Lorentzian shifts proportionally to the external magnetic field, explaining the magnetic field dependence of DNSP. The dark (light) gray curve show the situation at the critical field B_1^c (B_2^c). The figure illustrates that: 1.) Bistability can only be observed if the maximal slope of the Lorentzian is bigger than 1 and 2.) the difference between B_1^c and B_2^c is on the order of the width of the electron spin states in units of magnetic fields $\hbar/\tau_{el}g^*_{el}\mu_B$. (b) Total magnetic field B_{tot} seen by the QD electron under optical orientation of nuclear spins with σ^+-polarized light (gray curve). The curve is calculated from (1.17) with the parameters found from the fit presented in Fig. 1.5. The model shows that when the nuclear magnetic field B_{nuc} opposes the external field (i.e., for $0 < B_{ext} < 1.74$ T), the nuclei overcompensate B_{ext} and the electron sees a total magnetic field $B_{tot} < 0$. When the nuclear field saturates to its highest value, B_{tot} is very close to zero and the nuclear spin polarization becomes unstable

high degree of nuclear polarization, reaching OS_{max} at its maximum, while the other one shows a low degree of nuclear polarization. The graphical solution also shows that bistability is an inherent property of the solutions of (1.17) for systems where OS_{max} is at least on the order of the width of the density of states of the electronic spins ($\hbar/\tau_{el}$), which is typically the case for localized carriers such as in QDs, but not for bulk systems. The two stable solutions can be understood as follows: When increasing an external field while creating a nuclear field in the opposite direction, the electron Zeeman splitting is reduced compared to the case where nuclear spin polarization is absent. Therefore, the nuclear spin relaxation rate T_{1e}^{-1} remains at a high value such that DNSP can be maintained. As soon as OS_{max} is reached, however, the system can no further compensate for an increasing external magnetic field. DNSP will start to drop, which eventually leads to an abrupt jump of DNSP to a low value at an external field B_1^c. This jump is due to the negative feedback of DNSP on T_{1e}^{-1}. When ramping the external field down again, now in the absence of nuclear polarization, the system will initially remain in a state of low DNSP since T_{1e}^{-1} is still low. At the same time, DNSP will slightly increase due to the increasing

rate T_{1e}^{-1} of nuclear polarization with decreasing magnetic field strength. At a field B_2^c, the positive feedback of increasing DNSP on T_{1e}^{-1} will take over and an abrupt jump to a state of high nuclear polarization will occur. As can be seen from Fig. 1.6(a), the difference between the fields B_1^c and B_2^c is on the order of the width of the electronic spin states in units of magnetic fields.

In order to observe the hysteretic behavior of DNSP we performed a magnetic field dependent PL experiment as described above, now by exciting the QD with light of constant helicity and by ramping the magnetic field from low to high values and back again. Hysteretic behavior can be expected if the nuclear fields created in that way are pointing against the external magnetic field. In our system such a situation is realized when exciting the QD with σ^+ light and applying an external field in the positive z-direction.

Figure 1.7 shows data obtained in this regime: Going from low to high field amplitude, DNSP is significant up to a magnetic field of $B_1^c = 1.74$ T, where it suddenly drops. Sweeping the magnetic field back to low field amplitudes, DNSP reappears at a field $B_2^c = 1.36$ T, a value different from B_1^c. The difference of 380 mT between these two field is on the order of $\hbar/(\tau_{el} g_{el}^* \mu_B)$ as predicted by the model.

A fit of (1.18) to the data is also shown in Fig. 1.7. The parameters used for this fit were $T_{1e}^0/T_d = 3.5$, $\tau_{el} = 33$ ps, $g_{el}^* = -0.69$, consistent with the parameters used in the fit shown in Fig. 1.5. As in the previous fit, the residual nuclear polarization at high fields observed in this experiment is slightly higher than what is predicted by the model.

1.5.3 Discussion

We note that at the point of maximal Overhauser shift ($B_{ext} = B_1^c = 1.74$ T), our model predicts that B_{nuc} is almost completely cancelled by B_{ext} (see Fig. 1.6(b)). This point is therefore of particular interest because it enables a direct measure of the maximal nuclear field $B_{nuc}^{max} = OS_{max}/g\mu_B = B_1 = 1.74$ T. Remarkably, the remaining exciton Zeeman splitting at this point is solely due to the Zeeman interaction of the hole with B_{ext}. We can therefore directly obtain the hole g-factor and find $g_h^* = -1.2$. This observation has found applications in the precise and systematic study of electron and hole g-factors in semiconductor QDs [47].

Our experiment along with the model also shows that the maximal nuclear polarization of $\sim 47\%$[11] achieved in our system is limited by the fraction T_d/T_{1e}^0, i.e., the ratio between nuclear spin decay time and electron mediated nuclear spin relaxation time. While T_d is a parameter given by the nature of the QD, T_{1e}^0 could potentially be modified by varying the pump power or the details of the excitation process [33].

[11] We estimate the degree of polarization by comparing $OS_{max} = 70$ μeV to the OS corresponding to full nuclear spin polarization, which was given in Sect. 1.3.3.

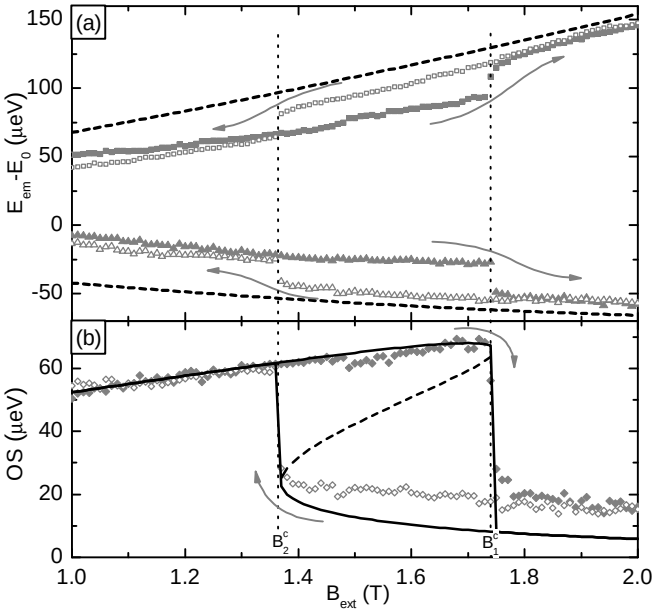

Fig. 1.7. Hysteresis behavior of the coupled electron-nuclear spin-system: Magnetic field sweeps under excitation with constant light polarization (σ^+). (a) Energy dispersion of X^{-1}, sweeping magnetic field up or down (as indicated by arrows). Squares (triangles) denote co- (cross-) circular detection with respect to excitation polarization. The dashed line is a fit to the case of linearly polarized excitation. (b) Overhauser shifts extracted from the data shown in (a) for the magnetic field sweeping up and down (solid and open diamonds, respectively). The black line shows the simulations described in the text

We extended the rate equation (1.16) and included the dynamics of the mean electron spin $\langle S_z \rangle$ by expanding (1.6) to first order in $\langle S_z \rangle$. The evolution of $\langle S_z \rangle$ is described by a rate equation similar to (1.17). The main differences between the electron and the nuclear spin dynamics are that the electron spin system, in the absence of other relaxation mechanisms, reaches the thermal equilibrium state (1.6) at a rate N/T_{1e}. Compared to the nuclear spin relaxation rate, the electron spin relaxation is faster by the number of nuclei N in the system. In addition, the electron spin is repumped into its initial state $S_z^0 = \rho_c^{\pm}/2$ at the exciton recombination rate on the order of 1 ns. This extension, however, did not lead to any new insights on the behavior of the nuclear spin system. A numerical study of this extended model suggested though that the mean value of the electron spin decreases linearly with increasing nuclear spin polarization. The electron spin thus seems to follow the intricate dynamics of the nuclear spin system. This observation motivates further studies on the positively charged exciton where PL light polarization gives a direct measure of the mean electron spin [48].

The qualitative disagreement of the model with our data in the low field regime where the measured DNSP shows a clear "kink" as a function of magnetic field indicates that our simple approach does not give a full description of the nonlinear processes that lead to an equilibrium value of DNSP in a QD. A further extension of the model could include light-induced nuclear spin relaxation due to the nuclear quadrupolar interaction [49] which could induce an additional loss of nuclear spin polarization at low external magnetic fields. Another possible nuclear depolarization mechanism relevant at low fields is the coupling of the nuclear Zeeman reservoir to the nuclear dipolar reservoir [28]. Since the heat conductivity for dipolar spin temperature is larger than for Zeeman spin temperature [50], the rate of nuclear spin depolarization in the QD will increase as soon as the two reservoirs couple. This coupling of nuclear Zeeman and dipolar reservoirs might therefore also explain the observed "kink" of DNSP at low fields. While our rate equation approach was purely classical, it could also be conceived that the quantum mechanical nature of the electron spin system would alter the behavior of DNSP at low fields and explain the unpredicted features in our measurement. In order to confirm this hypothesis further theoretical and experimental studies are required.

1.6 Buildup and Decay of Nuclear Spin Polarization

A key ingredient for the understanding of the coupled electron-nuclear spin system is the knowledge of the relevant timescales of the dynamics of nuclear spin polarization. This has already become apparent in Sect. 1.5, where (1.18) shows that the maximal nuclear spin polarization in a QD is limited by the ration of buildup and decay times of the nuclei. Many other aspects like the respective roles of nuclear spin diffusion, quadrupolar relaxation and trapped excess QD charges influence the dynamics of of DNSP and remain essentially unexplored up to now. While the buildup time of DNSP (τ_{buildup}) is likely to depend on the way the nuclear spin system is addressed, the DNSP decay time (τ_{decay}) is an inherent property of the isolated nuclear spin system of a QD. Furthermore, experimental determination of τ_{decay}, which directly yields the correlation time of the fluctuations of the Overhauser field along the axis in which the nuclei are polarized, can be crucial for understanding the limits of electron spin coherence in QDs [17].

In order to study the buildup and decay of DNSP, we extended our standard μPL setup (Sect. 1.2) by the ability to perform "pump-probe" measurements. An acousto-optical modulator (AOM) served as a fast switch of excitation light intensity, producing light pulses of variable lengths, with rise- and fall-times $\ll 1$ μs. We differentiate between "pump" pulses of duration τ_{pump}, used to polarize the nuclear spins, followed by "probe" pulses of length τ_{probe}, used to measure the resulting degree of DNSP. The intensity of each pulse corresponds to the saturation intensity of the observed emission line, maximizing both the resulting OS and the signal to noise ratio (SNR) of the

measurement. A mechanical shutter placed in the PL collection path is used to block the pump pulses while allowing the probe pulses to reach the spectrometer. Pump and probe pulses are separated by a waiting time τ_{wait} with a minimal length of 0.5 ms, limited by the jitter of the shutter opening time. In order to measure the buildup (decay) time of DNSP, τ_{pump} (τ_{wait}) are varied, respectively, while keeping all other parameters fixed. The timing and synchronization of the pulses is computer controlled via a digital acquisition card operating at a clock period of 2 μs, which sets the time resolution of the pulse sequences. Individual pump-probe sequences are repeated while the signal is accumulated on the spectrometer CCD in order to obtain a reasonable SNR. We verify a posteriori that individual pump-probe pairs are separated by much more than the measured DNSP decay time.

Figure 1.8(b) and (c) show the results for buildup and decay curves of DNSP obtained with this technique. The resulting curves fit surprisingly well to a simple exponential, yielding $\tau_{\mathrm{buildup}} = 9.4$ ms and $\tau_{\mathrm{decay}} = 1.9$ ms[12]. The small residual OS observed for $\tau_{\mathrm{pump}} = 0$ ($\tau_{\mathrm{wait}} \gg \tau_{\mathrm{decay}}$) in the buildup (decay) time measurement is due to the nuclear polarization created by the probe pulse. Comparing our experimental findings to previous experiments is not straightforward, since, to the best of our knowledge, the dynamics of DNSP at zero external magnetic field has not been studied up to now. However, in experiments performed at external magnetic fields of ~ 1 T, the buildup time of DNSP in QDs was estimated to be on the order of a few seconds [19, 42]. A further shortening of τ_{buildup} could arise from the strong localization of carriers in our QDs, which has been shown to be an important ingredient for efficient nuclear spin polarization [31]. Most strikingly, previous experimental results in similar systems revealed DNSP decay times on the order of minutes [30]. It is thus at first sight surprising that we find a DNSP decay time as short as a few milliseconds.

1.6.1 Electron mediated nuclear spin decay

A possible cause for the fast decay of DNSP is the presence of the residual QD electron even in the absence of optical pumping. We study its influence on τ_{decay} with the following experiment: While the nuclear spin polarization is left to decay, we apply a voltage pulse to the QD gate electrodes, ejecting the residual electron from the QD into the nearby electron reservoir. This is achieved by switching the QD gate voltage to a value where the dominant spectral feature observed in PL stems from the recombination of the neutral exciton. Using transient voltage pulses, we are able to perform this "gate voltage switching" on a timescale of 30 μs. Before sending the probe pulse onto

[12]The rate equation model presented in Sect. 1.5 predicts deviations from an exponential dependance due to the feedback of DNSP on the nuclear spin cooling rate. However, the limited SNR of our experiment and the finite length of the probe pulses do not allow us to observe these deviations at zero magnetic field.

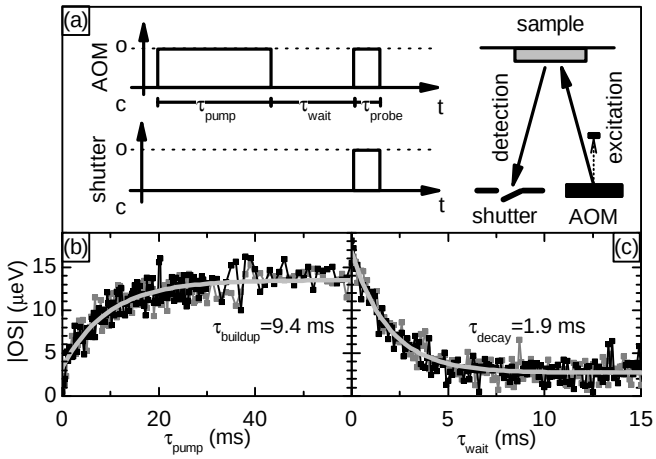

Fig. 1.8. (a) Schematic of the pulse sequences used in the buildup and decay time measurements of DNSP. An acousto optical modulator (AOM) deflects the excitation beam on and off the sample, serving as a fast switch (o (c) denote the open (closed) state, respectively). The AOM creates pump (probe) pulses of respective lengths τ_{pump} (τ_{probe}), separated by a waiting time τ_{wait}. A mechanical shutter blocks the pump pulse from reaching the spectrometer, while letting the probe pulse pass. (b) DNSP buildup curves obtained by varying τ_{pump} at fixed τ_{wait} (0.5 ms) and τ_{probe} (0.2 ms). The gray (black) data points correspond to QD excitation with light of positive (negative) helicity. The light gray line is an exponential fit, yielding a buildup time of $\tau_{\mathrm{buildup}} = 9.4$ ms. (c) DNSP decay curves obtained by varying τ_{wait} at fixed τ_{pump} (50 ms) and τ_{probe} (0.5 ms). The color coding is identical to (a). The exponential fit reveals a decay time of $\tau_{\mathrm{decay}} = 1.9$ ms

the QD, the gate voltage is switched back to its initial value in order to collect PL from X^{-1} recombination. The dramatic effect of this gate voltage pulsing on DNSP lifetime is shown in Fig. 1.9(b). On the timescale of the previous measurements, almost no DNSP decay can be observed. By prolonging τ_{wait} up to a few seconds (Fig. 1.9(c)), we estimate the spin decay time of the unperturbed nuclear system to be $\tau_{\mathrm{decay}} \approx 2.3$ s. We note that the increase of τ_{wait} necessary for this experiment results in a reduced SNR, which makes an exact determination of τ_{decay} difficult.

The role of the residual electron in depolarizing the nuclear spins was further confirmed in two independent measurements (not shown here). First, we perform a modified version of the gate voltage switching experiment: During the interval τ_{wait}, the gate voltage is switched to a regime where the QD ground state consists of two electrons in a spin singlet state [51]. This state doesn't couple to the nuclear spins and the measured τ_{decay} is again on the order of seconds. The second control experiment consists in measuring DNSP dynamics at a constant gate voltage where X^{+1} is the stable QD charge complex. As we showed in Sect. 1.4, optically pumping the X^{+1} exciton can also

lead to DNSP. However, in this case, the optically created electron polarizes the nuclear spins and no electron is left in the QD after exciton recombination. The corresponding DNSP decay channel is therefore not present. As expected, τ_{decay} is also on the order of seconds for this case.

We argue that two mechanisms could lead to the efficient decay of DNSP due to the residual electron. The first mechanism is caused by the randomization of the residual QD electron spin through co-tunnelling to the close-by electron reservoir. Co-tunnelling happens on a timescale of $\tau_{\mathrm{cot}} \approx 3$ ns for the structure studied in this work [26]. The resulting electron spin depolarization is mapped onto the nuclear spin system via hyperfine flip-flop events. Taking into account the detuning $\Delta E_{\mathrm{el}}^{\mathrm{Z}}$ of the two electron spin levels and using (1.15), the nuclear spin depolarization rate can be estimated to be $T_{1\mathrm{e}}^{-1} \simeq (A/N\Delta E_{\mathrm{el}}^{\mathrm{Z}})^2/\tau_{\mathrm{cot}}$ [35]. In order to get a rough estimate of the resulting timescale, we take $\Delta E_{\mathrm{el}}^{\mathrm{Z}}$ to be constant and equal to half the maximum measured OS. With these values, we obtain a nuclear spin depolarization time on the order of 100 ms, roughly consistent with our measurement.

A second possible mechanism is the indirect coupling of nuclear spins due the presence of a QD (conduction band) electron [27]. While this process conserves the total angular momentum of the nuclear spin system, it can lead to a decay of the OS by re-distributing the nuclear spin polarization within the QD and by increasing the nuclear spin diffusion rate out of the QD. The resulting decay rate for the nuclear field has been estimated to be on the order of $T_{\mathrm{ind}}^{-1} \simeq A^2/N^{3/2}\Delta E_{\mathrm{el}}^{\mathrm{Z}}$ as discussed in Sect. 1.3.4. The corresponding estimate for τ_{decay} of ~ 1 ms was obtained in the limit of $\Delta E_{\mathrm{el}}^{\mathrm{Z}} \gg A$, which is the only regime where theoretical predictions for the timescale of indirect nuclear spin interactions in QDs are available.

Our study of DNSP timescales was complemented by adding a permanent magnet to our sample. The resulting magnetic field is antiparallel to the excitation beam direction and has a magnitude of $B_{\mathrm{ext}} = -220$ mT at the site of the QD. The buildup and decay time measurements in the presence of B_{ext} are shown in Fig. 1.10. In accordance with the discussion of Sect. 1.5, an asymmetry between the cases of σ^+ and σ^- excitation is observed. The situation where B_{nuc} opposes B_{ext} is more efficient than the one where B_{nuc} aligns with B_{ext}; equilibrium is therefore reached faster and at a higher nuclear spin polarization in the first case, which corresponds to σ^--excitation for the present magnetic field direction. The measurements presented in Fig. 1.10(a) and (b) confirm this picture: we find that τ_{buildup} and τ_{decay} are both increased by a factor of $\sim 2-3$ when the polarization of the excitation light is changed from σ^- to σ^+.

We again performed the "gate voltage switching" experiment in the presence of B_{ext} (Fig. 1.10(c)). Since in this case DNSP decay is not mediated by the residual QD electron, no dependance of τ_{decay} on excitation light helicity was found and only the average between the two data sets (σ^+ and σ^- excitation) is shown. Compared to the case of zero external magnetic field, the decay of nuclear spin polarization is further suppressed. Even though extract-

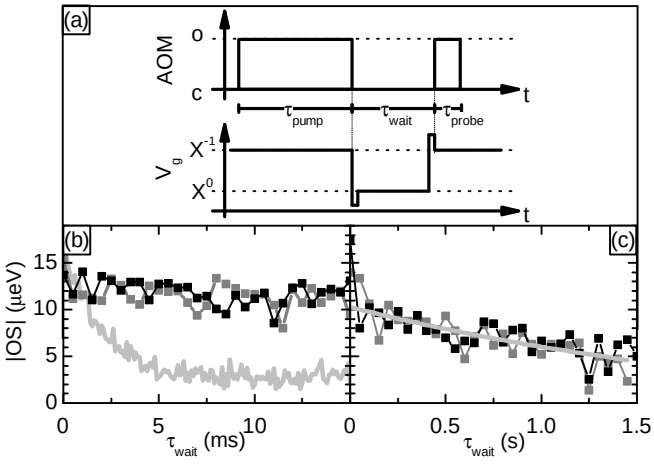

Fig. 1.9. (a) Timing diagram for the gate voltage switching experiment: During the period $\tau_{\rm wait}$, the QD gate voltage is switched to a value where the neutral exciton is the stable QD charge complex. Using transient pulses, the switching time is 30 μs. Ejecting the residual QD electron removes its effect on DNSP depolarization. This is demonstrated in (b), which shows DNSP decay measurements in the absence of the residual QD electron. The gray (black) data points represent DNSP decay under σ^+ (σ^-) excitation. For comparison, the light gray curve shows the mean of the data presented in Fig. 1.8(b). (c) Same measurement as in (b), but over a longer timescale. The exponential fit (light gray) indicates a decay time constant of $\tau_{\rm decay} \approx 2.3$ s

ing exact numbers is difficult in this case due to the required long waiting times, we estimate $\tau_{\rm decay}$ to be on the order of a minute. This further suppression of DNSP decay rate can be induced with a magnetic field as small as $\sim$ 1 mT as shown in the inset of Fig. 1.10(c): Keeping $\tau_{\rm wait} = 1$ s fixed, we sweep an external magnetic field while measuring the remaining OS. The resulting dip around $B_{\rm ext} = 0$ has a half-width of $\sim$ 1 mT. This indicates that nuclear spin depolarization at zero magnetic field is governed by the non-secular terms of the nuclear dipole-dipole interactions (1.4) which can be suppressed by applying an external magnetic field that exceeds the local dipolar field $B_{\rm loc} \approx 0.1$ mT [35]. The exact nature of this zero field decay of DNSP, however, is still unclear since nuclear dipole interactions should depolarize the nuclear spins in a much shorter time on the order of $T_2 \approx 10 - 100$ μs. We suggest that the interplay of dipolar interactions and quadrupolar shifts could explain this experimental results at low magnetic fields.

We also investigated the possible role of nuclear spin diffusion and the resulting DNSP of the bulk nuclei surrounding the QD. For this purpose, we studied the dependance of $\tau_{\rm decay}$ on the nuclear spin pumping time $\tau_{\rm pump}$ for $\tau_{\rm pump} \gg \tau_{\rm buildup}$ in the absence of the QD electron. A nuclear spin polarization in the surrounding of the QD would lead to an increase of $\tau_{\rm decay}$ with increasing $\tau_{\rm pump}$ [30]. However, within the experimental parameters accessible

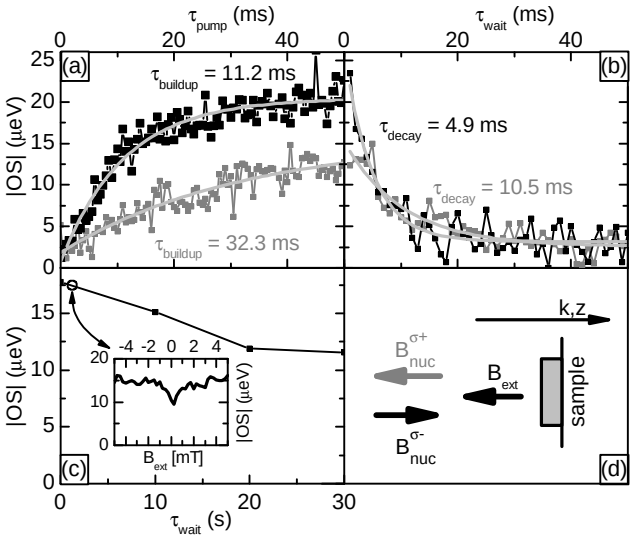

Fig. 1.10. Measurements of buildup and decay of DNSP in an external magnetic field $B_{\rm ext} \approx -220$ mT: (a) Buildup of DNSP. In the presence of $B_{\rm ext}$, it is more efficient and thus faster to produce a nuclear magnetic field compensating the latter (black, σ^- excitation) than one that enforces it (gray, σ^+ excitation). (b) If DNSP decay is mediated through the residual QD electron, it is again more efficient to depolarize the nuclei if the total effective magnetic field seen by the electron is minimized. The color coding is the same as in (a). Solid curves in (a) and (b) show exponential fits to the data, the resulting buildup- and decay times are given in the figures. (c) Decay of DNSP in the absence of the QD electron. Compared to the zero-field case (Fig. 1.9(c)), DNSP decay time is prolonged to $\tau_{\rm decay} \approx 60$ s. The inset shows OS after a waiting time of $1s$ as a function of external magnetic field. DNSP decay is suppressed on a magnetic field scale of ~ 1 mT, indicative of DNSP decay mediated by nuclear dipole-dipole interactions. (d) shows the respective directions of the external magnetic field and the nuclear fields $B^{\sigma^+}_{\rm nuc}$ ($B^{\sigma^-}_{\rm nuc}$) induced by QD excitation with σ^+ (σ^-) polarized light

with our experiment, we were unable to see such a prolongation and hence any effect of polarization of the surrounding bulk nuclei. We interpret this fact as a strong indication that we indeed create and observe a very isolated system of spin polarized nuclei. The QD boundaries constitute a barrier for spin diffusion and the small remaining flux of nuclear spin polarization is too low to saturate the bulk material surrounding the dot.

Finally, we note that we have tested the dependance of our experimental results on the polarization of the probe pulse. We repeated all experiments presented in this section using probe pulses both with linear polarization or with orthogonal polarization with respect to the pump pulse. This test revealed that our experimental findings are independent of the polarization of the pump pulse. While for experiments performed in the presence of an

external magnetic field this shows that our probe pulses indeed does not alter the nuclear spin polarization, this observation is surprising for experiments in zero magnetic field. As we discussed in Sect. 1.3.2, in the absence of external magnetic fields, nuclear spin polarization is destroyed on a timescale $T_2 \approx 10 - 100\ \mu$s by nuclear dipole-dipole interactions. At the same time, nuclear spin temperature has a lifetime $T_1 \gg T_2$, even at zero magnetic field (see [35], Chap. 5). In Sect. 1.4, we explained our experimental observation of DNSP at zero field with the presence of a relatively strong Knight field during optical pumping of QD nuclear spins. Since this Knight field is zero in the absence of laser excitation, one would expect DNSP to decay within a time T_2 after switching off the pump pulse. The probe pulse arriving after τ_{wait} (with $T_2 < \tau_{\mathrm{wait}} < T_1$) would then lead to the reappearance of DNSP oriented along the Knight field created by the probe pulse, which is opposite to the Knight field of the pump pulse if the helicity was switched between the pump and the probe pulse. The fact that we do not see the corresponding reversal of the sign of DNSP indicates that the nuclear T_2 time is on the order of T_1 for the QD nuclear spin system. A possible reason for this could be the strong nuclear quadrupolar interactions in QDs [52] which can partly suppress the effect of nuclear dipole-dipole interactions [53].

1.6.2 High Field Nuclear Spin Dynamics

In view of the nonlinear coupling between the electron and the nuclear spin system that was demonstrated in Sect. 1.5, the purely exponential buildup and decay curves measured in Sect. 1.6 might come as a surprise. Since the nuclear spin relaxation rate $T_{1\mathrm{e}}$ due to the QD electron depends on electron spin detuning, the buildup and decay rates of DNSP should depend on the degree of nuclear spin polarization and therefore change during the time traces presented in Fig. 1.8. These nonlinear effects are most prominent at the moment where the external and nuclear magnetic fields cancel. Since at low external magnetic fields this corresponds to the regime of almost zero nuclear spin polarization (i.e., to the beginning of the buildup- resp. to the end of the decay-curves), the experimental signature of the nonlinear character of the electron-nuclear spin system is not very pronounced there.

When increasing the external magnetic field, the nuclear spin dynamics slow down due to the increasing electron Zeeman splitting. However, in a configuration where B_{nuc} opposes B_{ext}, the total magnetic field felt by the QD electron crosses through zero at some point during the buildup and the decay of DNSP (cf. Fig. 1.6). At this point, the nuclear spin dynamics speed up again and $T_{1\mathrm{e}} = T_{1\mathrm{e}}^0$.

In order to observe the nonlinear buildup and decay curves discussed above, we performed the pump-probe measurement of DNSP described earlier in a regime of positive magnetic field and with excitation light of positive helicity (σ^+). Additionally, the nuclear spin polarization is reset between every pump-probe pulse pair by illumination with linearly polarized light for

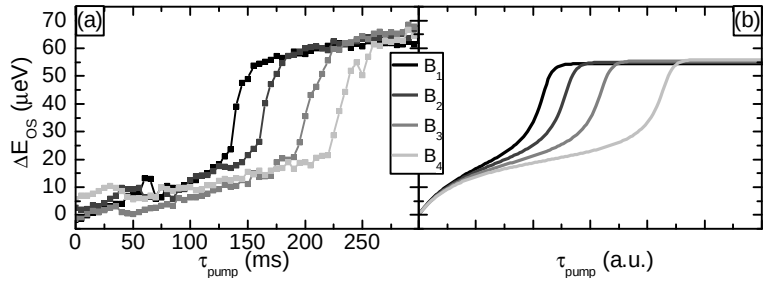

Fig. 1.11. (a) Buildup of DNSP in external magnetic fields on the order of the Overhauser field. The experiment was performed with the procedure and external parameters described in the main text at magnetic fields $B_1 = 1.1$ T, $B_2 = 1.2$ T, $B_3 = 1.3$ T and $B_4 = 1.4$ T. (b) Simulations according to the classical nonlinear rate equation (1.17) with the parameters found in the fit for Fig. 1.5. The magnetic fields used for the simulation are $B_1 = 1.22$ T, $B_2 = 1.24$ T, $B_3 = 1.26$ T and $B_4 = 1.28$ T.

100 ms. This ensures that individual pump-probe sequences are independent of each other.

Figure 1.11 shows the buildup curves of DNSP measured at various external magnetic fields. The nonlinear effects discussed before are clearly visible in this measurement. Also shown in the figure is a numerical simulation of the dynamics described by the nonlinear equation of motion (1.17) at the corresponding magnetic fields. The parameters for these curves are directly taken from the fit to the data presented in Fig. 1.5 without any further adjustments[13]. We note that the magnetic fields applied in the measurement do not completely agree with the magnetic fields used in the simulation. This is most probably due to slightly different excitation conditions (in terms of excitation power and energy) between this experiment and the one presented in Sect. 1.5. Changing these parameters can significantly alter the critical magnetic fields $B^{\mathrm{c}}_{1,2}$ defined in Sect. 1.5 and therefore the magnetic field dependance of the buildup of DNSP.

A much more interesting situation arises for the decay of DNSP in sizable external magnetic fields. Since the nuclear spin decay rate depends strongly on the electronic environment of the nuclei, the dependance on $\Delta E^{\mathrm{Z}}_{\mathrm{el}}$ of the electron-mediated DNSP decay rate can have various forms, depending on the relative importance of the different possible mechanisms discussed in Sect. 1.6.1.

A good picture of the different decay characteristics at various QD gate voltages in high magnetic fields can be obtained by measuring DNSP simultaneously as a function of gate voltage and time. The nuclei are initialized in a state of maximal DNSP at a gate voltage V_1 corresponding to the center of

[13]Since these fits only gave the relative time-constants of buildup and decay but not their absolute values, the time axis in Fig. 1.11(b) is given in arbitrary units.

the X^{-1} plateau. The gate voltage is then switched to a value V_2 and DNSP is measured after a waiting time τ_{wait}. In this measurement we scan τ_{wait} first and step to the next value in V_2 after a full time trace is recorded. The measurement result as a function of V_2 and τ_{wait} is shown in Fig. 1.12(a), where the final degree of DNSP is encoded in gray-scale. The voltages corresponding to the crossover between the (n)- and $(n+1)$-electron regimes as determined from a gate voltage dependant PL experiment (at the lowest possible excitation power) are marked in the figure[14]. In agreement with the discussion in Sect. 1.6, the measurement shows three clearly distinct regions of DNSP decay: When the QD is occupied by a single electron, DNSP decays in tens of ms; when zero or two electrons are present, there is no decay of DNSP on the timescale of the presented measurements. Even when increasing the measurement time to 5min, DNSP shows virtually no decay in these regions. We speculate that the corresponding nuclear T_1 time is on the order of hours.

In the region where the QD is occupied with one electron, the fast DNSP decay shows a much richer behavior. The decay rate shows a marked increase when V_2 approaches the edge of the $1e^-$-plateau, where co-tunnelling rates increase substantially [26]. This illustrates the importance of co-tunneling in electron-mediated DNSP decay, which is twofold: Co-tunneling ensures that the mean electron spin polarization is zero due to the coupling to the (unpolarized) electron reservoir; this sets the equilibrium nuclear spin polarization through (1.6). Furthermore, co-tunneling limits the electron spin correlation time τ_{el}, which broadens the electron spin states and allows for electron-nuclear spin flips to happen at first place.

When approaching the $1e^-$-$2e^-$ transition point however ($0.02V < V_2 < 0.04V$), nuclear spin lifetime increases again, even though the stable configuration of the QD is still singly charged. We believe that this is a signature of motional narrowing: While a finite τ_{el} is necessary to overcome the energy mismatch of the initial and final states of an electron-nuclear spin flip-flop, the nuclei cannot undergo such a transition if the electron spin fluctuations become too fast. This becomes apparent by inspecting (1.15) which shows that T_{1e} has a maximum for $\tau_{\text{el}} = 1/\Omega_{\text{el}}$. We observe the maximal electron-nuclear spin relaxation rate at a gate voltage $V_2 = 0.02$ V. Since at $\tau_{\text{wait}} = 0$ the total electron Zeeman splitting ($\Delta E_{\text{OS}} + g^*_{\text{el}}\mu_B B_{\text{ext}}$) amounts to ~ 20 μeV, the corresponding electron co-tunnelling rate at this gate voltage is on the order of 30 GHz, consistent with independent calculations of this quantity [26]. Motional narrowing is not observed on the $0e^-$-$1e^-$ transition, where one would at first sight expect a similar behavior as in the $1e^-$-$2e^-$ transition since co-tunneling processes are equivalent for these two regimes. However, this is not strictly true since the tunneling rate also has a dependance on gate voltage

[14] We note that these voltages do not correspond to the voltages indicated in Fig. 1.1. The reason for this is light-induced accumulation of space-charges in our gated structures during laser excitation. These charges screen the applied gate voltage, thereby shifting it to lower values.

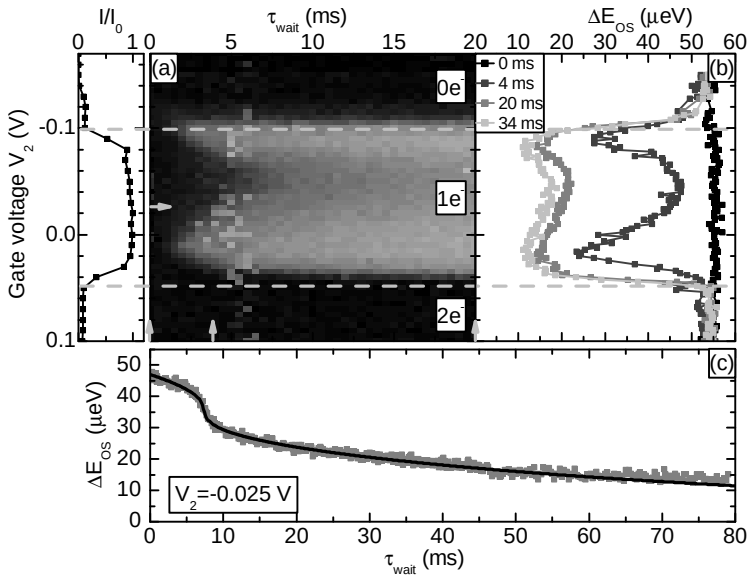

Fig. 1.12. Decay of DNSP in an external magnetic field of $B_{\rm ext} = 1$ T. The nuclear spin polarization was initialized with a 100 ms, σ^+-polarized pump pulse at a gate voltage V_1 corresponding to the middle of the $1e^-$-plateau, resulting in an initial Overhauser shift $\Delta E_{\rm OS}(0) \approx 55$ μeV. Immediately after this nuclear spin initialization, the gate voltage was switched to a value V_2. (a) Measurement of $\Delta E_{\rm OS}$ as a function of waiting time $t_{\rm wait}$ and gate voltage V_2. Gray lines indicate the transition between the QD charging states identified by the low power PL experiment shown in the left panel. (b) and (c) are line-cuts through figure (a) at fixed $t_{\rm wait}$ and V_2, respectively, as indicated by the gray arrows in (a) ((a), (b) and (c) have all been obtained by independent measurements). The black line in (c) is a fit according to (1.17)

and increases exponentially with increasing voltage. Therefore, co-tunneling is slower on the $0e^-$-$1e^-$ transition than on the $1e^-$-$2e^-$ transition and $\tau_{\rm el}$ never reaches the value $1/\Omega_{\rm el}$ on the low-voltage side of the $1e^-$-plateau.

The center of the $1e^-$-plateau shows a lifetime of DNSP of roughly 10 ms, limited by the interactions of the QD nuclei with the residual QD electron which is randomized by co-tunnelling with the reservoir. Due to the nonlinear electron-nuclear spin coupling, the decay in this region shows a highly nonlinear behavior as presented in Fig. 1.12(c). Nuclear spin depolarization initially happens at a rather slow rate but speeds up as soon as $B_{\rm nuc}$ and $B_{\rm ext}$ cancel after $t_{\rm wait} \approx 7$ ms and at $\Delta E_{\rm OS} \approx 36$ μeV. Once $|B_{\rm nuc}| < |B_{\rm ext}|$, the electron Zeeman splitting increases again and DNSP decay slows down. We fitted the measured decay curve by a numerical solution of the rate equation (1.16) for $S_z = 0$ and an initial condition $\Delta E_{\rm OS}(0)$. The parameters found in this fit were $\Delta E_{\rm OS}(0) = 47$ μeV, $T_{1\rm e}^0 = 3.3$ ms, $T_{\rm d} = 110$ ms, $\tau_{\rm el} = 360$ ps and $g_{\rm el}^* = -0.62$,

in agreement with the corresponding numbers found in Sect. 1.5.2. However, the electron spin correlation time we found is surprisingly short given that the measurement was performed in the absence of optical excitation. Even though, this measurement of DNSP decay was not performed exactly at the center of the $1e^-$-stability plateau (cf. Fig. 1.12(a)), we would expect τ_{el} to be on the order of 1 ns. Another surprising feature is the remaining nuclear spin depolarization time of $T_{\mathrm{d}} = 110$ ms. We note that this nuclear spin relaxation cannot be due to spin diffusion mediated by nuclear dipole-dipole interactions, since this rate has to be much smaller given the long DNSP lifetime indicated by the measurement in the $0e^-$- and $2e^-$-regions of Fig. 1.12(a). The mechanism causing nuclear spin relaxation at the rate $T_{\mathrm{d}}^{-1} \approx 0.1$Hz must therefore be caused by the presence of the residual QD electron. We believe that indirect nuclear spin interactions mediated by the QD electron cause this decay through the mechanism discussed in Sect. 1.3.4. This decay is not expected to be exponential and further study of the DNSP decay dynamics in this regime is required to fully understand the measurement presented in Fig. 1.12(c).

A surprising feature arises in the transition between the $1e^-$ and $0e^-$ regimes ($-0.14V < V_2 < -0.1V$). Fig. 1.12(b) shows that in this regime DNSP has an initial, fast decay (on a timescale $\ll 1$ ms, not resolved in this measurement) after which it settles at a finite value of DNSP and shows no further decay on the timescale of our experiments. This unexplained observation is very surprising since it occurs in a regime where the QD is in a neutral state and only virtual occupations by a single electron are allowed. Furthermore, DNSP decay seems to stop at a value where the total electron Zeeman splitting is smaller than its value at $\tau_{\mathrm{wait}} = 0$ and where one would therefore expect DNSP decay to be enhanced. Understanding the interesting dynamics in this QD charging regime requires further investigation.

We note that we have repeated the experiment discussed above for external magnetic fields of $B_{\mathrm{ext}} = 0$, 0.5 and 1.5 T. The basic features described above have been observed at all those fields. At $B_{\mathrm{ext}} = 0$, DNSP decay in the $1e^-$-region is too fast to observe a variation of co-tunnelling rates over the $1e^-$-stability plateau. We also checked the dependance of our results on the exact form of the gate voltage-overshoots used to switch V_g between V_1 and V_2 (cf. Fig. 1.9) and found that the gate voltage-switching does not influence our results. A further check for the validity of our results was to change the order in which τ_{wait} and V_2 were measured. Sweeping V_2 and stepping τ_{wait} gave results identical to the ones depicted in Fig. 1.12.

We conclude that we have good understanding of the decay dynamics of DNSP in the regimes where the QD electron occupancy number is well defined. In the cross-over regions where the QD charging state is changed, DNSP decay shows unexpected features that warrant further investigation.

1.7 Future perspectives

One of the principal experimental findings presented in this work was the identification of the QD electron as an efficient source of nuclear spin decay. While in our approach the electron is indispensable for building up a nuclear spin polarization in the first place, it also acts against this buildup by inducing indirect nuclear spin interactions as well as co-tunnelling mediated depolarization. In order to increase the maximal attainable degree of nuclear spin polarization it would therefore be interesting to investigate possibilities of suppressing this electron-mediated DNSP decay. This could be achieved by increasing the tunnelling barrier between the QD and the electron reservoir in our structures. However, changing this parameter also has the consequence of changing the electron spin correlation time τ_{el} and the fraction of QD electron occupation, f_{el}. Both these factors crucially influence the QD nuclear spin dynamics in various ways. Systematically studying the dependance of DNSP on the QD tunneling barrier thickness could therefore yield valuable information on how to enhance DNSP in self-assembled QDs.

For the interpretation of all of our experimental results, considering the nuclear spins as an ensemble of classical magnetic moments was sufficient. Investigating their quantum mechanical nature would be interesting for both fundamental reasons and applications that aim at tailoring the fluctuations of the mean nuclear spin [7]. The back-action of a (quantum-mechanical) measurement of the nuclear spin polarization along a given axis would be an interesting experiment in this direction. In order to perform a projective measurement on the QD nuclear spin system, the accuracy of the detection of the Overhauser-shift has to be greatly improved as compared to our experimental technique. The necessary energy resolution for such an experiment has recently been estimated to be on the order of $A/N^{3/2}$ [7]. Using optimistic numbers, this corresponds to an energy resolution of ~ 0.1 neV or ~ 25 kHz. While this resolution is out of reach with our present spectroscopic techniques, more advanced methods like optically detected electron spin resonance [54] or EIT [55] are close to reaching the required sensitivity. A first step in this direction would be the use of differential transmission measurements [56] to prepare and detect DNSP.

Our measurements of the Overhauser-shift of a QD electron give information about the mean nuclear field that the electron is exposed to. Investigating the role that the different nuclear species play in the dynamics of the nuclear field requires a further extension of our experimental techniques. Applying an NMR field resonant with a given nuclear spin species could induce additional heating for those spins, thereby giving information about the contribution of the different spin species to the measured Overhauser-shift. Such experiments are complicated by the large inhomogeneous broadening of the corresponding NMR lines caused by strain-induced quadrupolar shifts. Using more refined NMR and optical detection techniques, however, NMR experi-

ments could prove useful in investigating the dynamics of QD nuclear spins in greater detail.

Another exciting perspective is the experimental observation of the onset of nuclear order in a single QD. Different theoretical scenarios for these nuclear phase transitions have been proposed. Based on the experimental results presented in this work, realizing these proposals seems to be within experimental reach. Nuclear self polarization was predicted to occur for the case where nuclear spins couple to an electron spin system which is artificially maintained in a disordered spin state at sufficiently low electron temperatures [46]. Combining recent advances in electron spin resonance in self-assembled QDs [54] with the fast, non-invasive measurement of DNSP via pulsed PL could allow us to observe this spontaneous nuclear spin polarization which was predicted to occur at moderate temperatures of a few K. At much lower temperatures, a true ferromagnetic phase transition of the nuclear spins was recently predicted to occur in semiconductor nano-structures [57]. A possibility for reaching low nuclear spin temperatures in the μK range is adiabatic demagnetization of QD nuclear spins. Bringing the optically cooled nuclear spin system from a field on the order of 1 T adiabatically to zero field could result in a nuclear spin temperature being $2-3$ orders of magnitude lower than what can be achieved through direct optical cooling.

Acknowledgements

We thank A. Badolato for crystal growth and J. Dreiser for help with sample preparation. P.M. would like to express his gratitude towards C.W. Lai who taught him the experimental techniques which made this work possible. Furthermore we acknowledge fruitful discussions with A. Högele, C. Latta and S.D. Huber. This work is supported by NCCR-Nanoscience.

References

1. A. Overhauser, Phys. Rev. **92**, 411 (1953)
2. G. Lampel, Phys. Rev. Lett. **20**, 491 (1968)
3. D. Paget, G. Lampel, B. Sapoval, V.I. Safarov, Phys. Rev. B **15**, 5780 (1977)
4. A.V. Khaetskii, D. Loss, L. Glazman, Phys. Rev. Lett. **88**, 186802 (2002)
5. A.C. Johnson, J.R. Petta, J.M. Taylor, A. Yacoby, M.D. Lukin, C.M. Marcus, M.P. Hanson, A.C. Gossard, Nature **435**, 925 (2005)
6. F.H.L. Koppens, J.A. Folk, J.M. Elzerman, R. Hanson, L.H.W. van Beveren, I.T. Vink, H.P. Tranitz, W. Wegscheider, L.P. Kouwenhoven, L.M.K. Vandersypen, Science **309**, 1346 (2005)
7. D. Klauser, W.A. Coish, D. Loss, Nuclear spin dynamics and zeno effect in quantum dots and defect centers (2008). URL arXiv:0802.2463v1
8. W.A. Coish, D. Loss, Phys. Rev. B **70**, 195340 (2004)
9. D. Gammon, S.W. Brown, E.S. Snow, T.A. Kennedy, D.S. Katzer, D. Park, Science **277**, 85 (1997)

10. S.W. Brown, T.A. Kennedy, D. Gammon, E.S. Snow, Phys. Rev. B **54**, R17339 (1996)
11. K. Ono, S. Tarucha, Phys. Rev. Lett. **92**, 256803 (2004)
12. A.S. Bracker, E.A. Stinaff, D. Gammon, M.E. Ware, J.G. Tischler, A. Shabaev, A.L. Efros, D. Park, D. Gershoni, V.L. Korenev, I.A. Merkulov, Phys. Rev. Lett. **94**, 047402 (2005)
13. B. Eble, O. Krebs, A. Lemaitre, K. Kowalik, A. Kudelski, P. Voisin, B. Urbaszek, X. Marie, T. Amand, Phys. Rev. B **74**, 081306 (2006)
14. C.W. Lai, P. Maletinsky, A. Badolato, A. Imamoglu, Phys. Rev. Lett. **96**, 167403 (2006)
15. A.I. Tartakovskii, T. Wright, A. Russell, V.I. Fal'ko, A.B. Van'kov, J. Skiba-Szymanska, I. Drouzas, R.S. Kolodka, M.S. Skolnick, P. Fry, A. Tahraoui, H.Y. Liu, M. Hopkinson, Phys. Rev. Lett. **98**, 26806 (2007)
16. I.A. Akimov, D.H. Feng, F. Henneberger, Phys. Rev. Lett. **97**, 056602 (2006)
17. I.A. Merkulov, A.L. Efros, M. Rosen, Phys. Rev. B **65**, 205309 (2002)
18. R.J. Warburton, C. Schaflein, D. Haft, F. Bickel, A. Lorke, K. Karrai, J.M. Garcia, W. Schoenfeld, P.M. Petroff, Nature **405**, 926 (2000)
19. P. Maletinsky, C.W. Lai, A. Badolato, A. Imamoglu, Phys. Rev. B **75**, 35409 (2007)
20. M. Bayer, G. Ortner, O. Stern, A. Kuther, A.A. Gorbunov, A. Forchel, P. Hawrylak, S. Fafard, K. Hinzer, T.L. Reinecke, S.N. Walck, J.P. Reithmaier, F. Klopf, F. Schäfer, Phys. Rev. B **65**, 195315 (2002)
21. M. Atatüre, J. Dreiser, A. Badolato, A. Högele, K. Karrai, A. Imamoglu, Science **312**, 551 (2006)
22. M.E. Ware, E.A. Stinaff, D. Gammon, M.F. Doty, A.S. Bracker, D. Gershoni, V.L. Korenev, S.C. Badescu, Y. Lyanda-Geller, T.L. Reinecke, Phys. Rev. Lett. **95**, 177403 (2005)
23. P.Y. Yu, M. Cardona, *Fundamentals of Semiconductors: Physics and Materials Properties*, 3rd edn. (Springer, Berlin, 2001)
24. M.J. Snelling, E. Blackwood, C.J. McDonagh, R.T. Harley, C.T.B. Foxon, Phys. Rev. B **45**, 3922 (1992)
25. S. Amasha, K. MacLean, I.P. Radu, D.M. Zumbühl, M.A. Kastner, M.P. Hanson, A.C. Gossard, Phys. Rev. Lett. **100**, 046803 (2008)
26. J.M. Smith, P.A. Dalgarno, R.J. Warburton, A.O. Govorov, K. Karrai, B.D. Gerardot, P.M. Petroff, Phys. Rev. Lett. **94**, 197402 (2005)
27. A. Abragam, *The principles of nuclear magnetism* (Clarendon Press, Oxford, 1961)
28. M. Goldman, *Spin Temperature and nuclear Magnetic Resonance in Solids* (Oxford University Press, 1970)
29. J.A. McNeil, W.G. Clark, Phys. Rev. B **13**, 4705 (1976)
30. D. Paget, Phys. Rev. B **25**, 4444 (1982)
31. A. Malinowski, M.A. Brand, R.T. Harley, Physica E **10**, 13 (2001)
32. I. Merkulov, Physics Uspekhi **45**, 1293 (2002)
33. P.F. Braun, B. Urbaszek, T. Amand, X. Marie, O. Krebs, B. Eble, A. Lemaitre, P. Voisin, Phys. Rev. B **74**, 245306 (2006)
34. E.I. Gryncharova, V.I. Perel, Sov. Phys. Semicond. **11**, 997 (1977)
35. F. Meier, *Optical orientation* (North-Holland, Amsterdam, 1984)
36. M.I. Dyakonov, V.I. Perel, Sov. Phys. JETP **38**, 177 (1974)
37. J.R. Petta, A.C. Johnson, J.M. Taylor, E.A. Laird, A. Yacoby, M.D. Lukin, C.M. Marcus, M.P. Hanson, A.C. Gossard, Science **309**, 2180 (2005)

38. G. Giedke, J.M. Taylor, D. D'Alessandro, M.D. Lukin, A. Imamoglu, Phys. Rev. A **74**, 032316 (2006)
39. D. Klauser, W.A. Coish, D. Loss, Phys. Rev. B **73**, 205302 (2006)
40. R. Hanson, L.P. Kouwenhoven, J.R. Petta, S. Tarucha, L.M.K. Vandersypen, Reviews of Modern Physics **79**, 1217 (2007)
41. W. Yao, R.B. Liu, L.J. Sham, Phys. Rev. B **74**, 195301 (2006)
42. D. Gammon, A.L. Efros, T.A. Kennedy, M. Rosen, D.S. Katzer, D. Park, S.W. Brown, V.L. Korenev, I.A. Merkulov, Phys. Rev. Lett. **86**, 5176 (2001)
43. V.L. Berkovits, C. Hermann, G. Lampel, A. Nakamura, Phys. Rev. B **18**, 1767 (1978)
44. S. Laurent, B. Eble, O. Krebs, A. Lemaitre, B. Urbaszek, X. Marie, T. Amand, P. Voisin, Phys. Rev. Lett. **94**, 147401 (2005)
45. E.L. Ivchenko, Pure Appl. Chem. **67**, 463 (1995)
46. M.I. Dyakonov, V.I. Perel, JETP Lett. **16**, 398 (1972)
47. R. Kaji, S. Adachi, H. Sasakura, S. Muto, Applied Physics Letters **91**, 261904 (2007)
48. R. Kaji, S. Adachi, H. Sasakura, S. Muto, Hysteretic response of electron-nuclear spin system in single inalas quantum dots:excitation power and polarization dependences (2007). URL arXiv:0709.1382
49. D. Paget, T. Amand, J. Korb, Light-induced nuclear quadrupolar relaxation in semiconductors (2008). URL arXiv:0801.2894v1
50. C. Ramanathan, Dynamic nuclear polarization and spin-diffusion in non-conducting solids (2008). URL arXiv.org:0801.2170
51. B. Urbaszek, R.J. Warburton, K. Karrai, B.D. Gerardot, P.M. Petroff, J.M. Garcia, Phys. Rev. Lett. **90**, 247403 (2003)
52. R.I. Dzhioev, V.L. Korenev, Phys. Rev. Lett. **99**, 037401 (2007). DOI 10.1103/PhysRevLett.99.037401. URL http://link.aps.org/abstract/PRL/v99/e037401
53. V. Kalevich, K. Kavokin, I. Merkulov. private communication (2008)
54. M. Kroner, K. Weiss, B. Biedermann, S. Seidl, S. Manus, A. Holleitner, A. Badolato, P. Petroff, B. Gerardot, R. Warburton, K. Karrai, Phys. Rev. Lett (2008)
55. A. Imamoglu, Phys. Stat. Sol. (b) **243**, 3725 (2006)
56. A. Hogele, M. Kroner, S. Seidl, K. Karrai, M. Atature, J. Dreiser, A. Imamoglu, R.J. Warburton, A. Badolato, B.D. Gerardot, P.M. Petroff, Appl. Phys. Lett. **86**, 221905 (2005)
57. P. Simon, D. Loss, Phys. Rev. Lett. **98**, 156401 (2007)